Palaeogeography, Palaeoclimatology, Palaeoecology 546 (2020) 109656

Contents lists available at ScienceDirect

Palaeogeography, Palaeoclimatology, Palaeoecology

journal homepage: www.elsevier.com/locate/palaeo

Palaeosalinity and palaeoclimatic geochemical proxies (elements Ti, Mg, Al) vary with Milankovitch cyclicity (1.3 to 2.0 Ma), OGCP cores, Palaeolake Olduvai, Tanzania

Ian G. Stanistreet[a,b,*], John F. Boyle[c], Harald Stollhofen[d], Daniel M. Deocampo[e], Alan Deino[f], Lindsay J. McHenry[g], Nicholas Toth[b], Kathy Schick[b], Jackson K. Njau[b,h]

[a] Dept. Earth, Ocean and Ecological Sciences, University of Liverpool, Brownlow Street, Liverpool L69 3GP, UK
[b] The Stone Age Institute, Bloomington, IN 47407-5097, USA
[c] Dept. Geography and Planning, School of Environmental Sciences, University of Liverpool, Liverpool, UK
[d] GeoZentrum Nordbayern, Friedrich-Alexander-University (FAU) Erlangen-Nürnberg, Schloßgarten 5, 91054 Erlangen, Germany
[e] Dept. Geosciences, Georgia State University, Atlanta, GA, USA
[f] Berkeley Geochronology Center, 2455 Ridge Road, Berkeley, CA 94709, USA
[g] Department of Geosciences, University of Wisconsin-Milwaukee, 3209 N. Maryland Ave., Milwaukee, WI 53211, USA
[h] Department of Earth and Atmospheric Sciences, Indiana University, 1001 East 10th Street, Bloomington, IN 47405-1405, USA

ARTICLE INFO

Editor: Thomas Algeo

Keywords:
Olduvai Basin
Precession
Obliquity
Orbital forcing
Basaltic magmatism
XRF scanning

ABSTRACT

The analysis of geochemical palaeoclimate and palaeosalinity proxy elements Ti, Mg, and Al, derived from X-ray fluorescence (XRF) scans of Olduvai Beds I and II from Olduvai Gorge Coring Project (OGCP) borehole Cores 2A and 3A, provides a record of cyclic variation between ~1.3 Ma and ~2.0 Ma. The boreholes were drilled into the depocentre of the Olduvai Basin between Fifth and FLK Faults, where Palaeolake Olduvai was most persistent and deepest. During most of Bed I the lake was particularly deep and probably meromictic, preserving high TOC contents and commonly preserving fine lamination due to lack of bioturbation. Accretion rates were also high during Bed I, when rates of basinal subsidence were maximal due to crustal stretching, associated with basaltic volcanism, towards the end of bimodal Ngorongoro volcanism. Basaltic magma effusive activity is manifested as tuffs, scoriaceous layers and the Bed I Basalt complex lava flows. A magnesium anomaly is recorded in the claystone geochemistry at this time and deposition of dolomite and limestone beds are restricted to this syn-volcanic phase of basin history. During Bed I deposition, accretion rates (0.23 mm/yr) were high enough to permit recognition of cycles with an average periodicity of 22.3 kyr corresponding to the Earth's precession. Only the high values during the Mg anomaly are adequate for the application of the palaeosalinity proxy element ratio Mg/Al. But Ti counts provide a cyclic record in both Bed I and Bed II. During Bed II deposition, the accretion rate was much slower (0.058 mm/yr) and cyclicity averaged 40.4 kyr, corresponding to Earth's orbital obliquity. The Bed II interval corresponds to MIS Stages 40 to 64. Coincidence of precessional and obliquity minima at 1.8 Ma explains the superdrought that affected the basin at the time of emplacement of Tuff IF, when the lake was dried out. The aridity of the sequence containing Tuff IA is also associated with a precessional minimum. The cyclic record suggests that three Bed I Basalt flows were extruded at ~1.94 Ma during a time span lasting between 6 kyr and 15 kyr.

1. Introduction

During August 2014, the Olduvai Gorge Coring Project (OGCP), under the auspices of the Stone Age Institute, drilled four boreholes at three sites (Fig. 1): 1A, 85 m; 2A, 245 m; 3A, 134 m; 3B, 147 m (the latter an inclined borehole drilled at the same site as 3A to facilitate palaeomagnetic reversal analysis) within the now extinct Palaeolake Olduvai. Located just west of the Ngorongoro Volcanic Highlands (NVH), the basin is filled with Pliocene-Pleistocene lake and interleaved fan-delta beds, unconformably overlying Neoproterozoic and Archaean gneissic metamorphic basement rocks. Original basin analysis was undertaken by Hay (1976), but subsequent studies related the basin-fill geometry to the syn-sedimentary structural framework that controlled sedimentation (Stollhofen and Stanistreet, 2012). According to the

* Corresponding author at: Dept. Earth, Ocean and Ecological Sciences, University of Liverpool, Brownlow Street, Liverpool L69 3GP, UK.
E-mail address: istanistreet@btconnect.com (I.G. Stanistreet).

https://doi.org/10.1016/j.palaeo.2020.109656
Received 20 May 2019; Received in revised form 7 February 2020; Accepted 8 February 2020
Available online 13 February 2020
0031-0182/

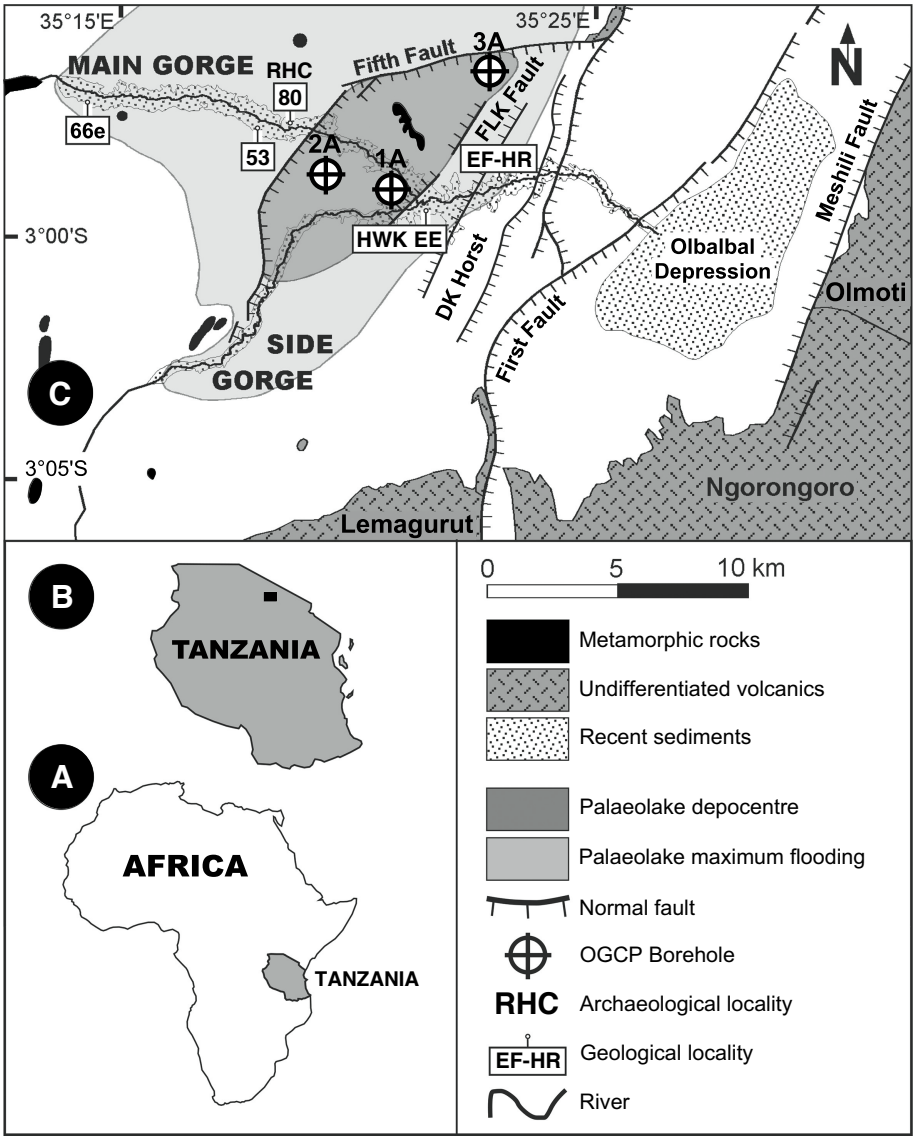

Fig. 1. Location of the three OGCP borehole sites and important geological/archaeological localities within the newly revealed depocentre of Palaeolake Olduvai, constrained between Fifth and FLK Faults. (Based on Hay, 1976).

latter, the basin could be considered to comprise two sub-basins: (i) that within the area of the present-day Olbalbal Depression, where subsidence was maximal, associated with the edge of the eastern branch of the African Rift System; and (ii) that between the FLK and Fifth Faults, representing the lake depocentre (Fig. 1). Between these two sub-basins is the DK Horst, and the basin was deduced to have subsided along an extensional detachment, Fifth Fault, with the DK Horst riding on the same detachment surface (Stollhofen and Stanistreet, 2012).

One major aim of the drilling campaign was to gain as complete a Palaeolake Olduvai core record as possible, to further the understanding of the palaeosalinity, palaeoenvironmental and palaeoclimatic history (see also Cohen et al., 2009). Because Hay (1976) had previously hypothesized that the depocentre of the lake had migrated eastwards during basinal depositional history, involving Beds I-IV, Masek, Ndutu and Naisiusiu Beds (Fig. 2), it was felt that multiple sites would be necessary to capture the full extent of lacustrine sequences. When the borehole cores were logged it was found that equivalent facies sequences could be correlated through all three drill sites (Stanistreet et al., this volume a), so that the lake was thus larger, deeper, more long-lived and more stably situated than previously perceived. Prior to its demise after the deposition of the Masek Beds, Palaeolake Olduvai was thus on a par with other, still extant East African rift valley lakes such as Lakes Eyasi (Stanistreet et al., this volume a).

Because Core 2A intersected best the central lacustrine facies of Upper Bed I and Bed II and Core 3A the central lacustrine facies of Beds I to IV and the Masek Beds (Fig. 3), the XRF scanned analyses of these two cores were selected as a key data set for the present palaeosalinity and palaeoclimatic study. Extending down to 245 m without reaching the basin floor, borehole core 2A more than doubled the known stratigraphy of the Olduvai Beds (Fig. 2), previously measured from outcrops to reach a maximum cumulative thickness of only ~100 m (Hay, 1976). Various tuff layers interbedded with lake beds provide a detailed tephrostratigraphic framework and multiple age calibration points. Previously, the oldest dated unit known was the Lower Bed I Naabi Ignimbrite, which yielded an $^{40}Ar/^{39}Ar$ date of 2.038 ± 0.005 Ma (Deino, 2012). But the drilling revealed 135 m of yet undated sub-Naabi basin stratigraphy. New formations defined (Fig. 2) are the Ngorongoro and Naibor Soit Formations (Stanistreet et al., this volume a). Major tephrostratigraphic units in Beds I to IV were named by Hay (1976) as Tuffs IA (Ngorongoro Volcano), IB to IF (Olmoti Volcano), IIA, IIB, IIIA, etc. Accordingly, Stanistreet et al. (this volume a) label major eruptive

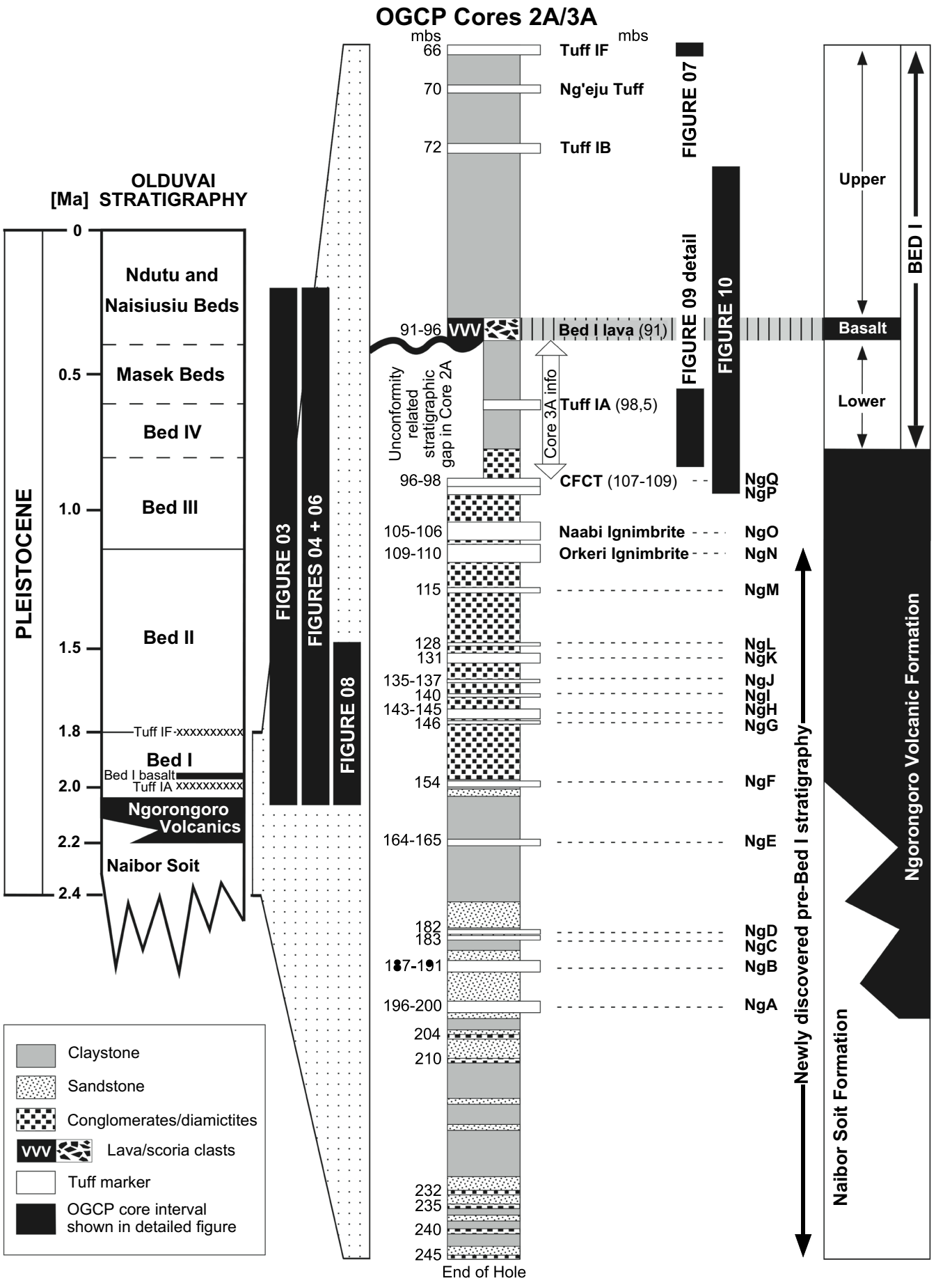

(caption on next page)

Fig. 2. Generalized Olduvai Basin stratigraphy (left column), based on Hay (1976) with middle stratigraphic column providing a combination of Core 2A and Core 3A stratigraphy considered in this paper. Most of the information is derived from Core 2A with numbers to the left of the stratigraphic column indicating mbs positions of marker beds. Only the CFCT to Bed I lava interval (marked by an arrow) is added from Core 3A (with mbs labels to the right of the column) as this interval is missing in Core 2A due to an unconformity. Notice newly discovered sub-Bed I strata (Naibor Soit and Ngorongoro Volcanic Formations) (Stanistreet et al., a, this volume) with NgA to NgQ labels indicating positions of marker tuffs in the Ngorongoro Formation (middle and right column). Black vertical bars illustrate stratigraphic positions of detailed figures.

events recorded within the Ngorongoro Formation as Tuffs NgA, NgB, NgC, … Tuff NgQ (Fig. 2), comprising 17 tephrostratigraphic units in all, most likely products of adjacent Ngorongoro Volcano. Applying average sediment accretion rates from the younger, well dated lake sequence, the older (sub-Naabi) stratigraphy takes the age of the Olduvai Beds back to ~2.4 Ma (Stanistreet et al., this volume a). At that depth, the earliest sediments, prior to the eruption of Ngorongoro Volcano, were found to be fluvio-lacustrine siliciclastics.

Thus, Palaeolake Olduvai was extant at least between ~2.4 Ma and 0.8 Ma (Stanistreet et al., this volume a) during the deposition of the Naibor Soit (lacustrine with fluvio-deltaics), Ngorongoro (fan-delta) Formations (Fig. 2), Beds I to IV (lacustrine with prograding fan-deltas) and the Masek (fan-delta) Beds. For the newly discovered pre-Bed I stratigraphy, the reader is directed to Stanistreet et al. (this volume a). Hay (1976) provides the basis for the stratigraphy younger than c. 2.0 Ma. After the Masek Beds, tectonic and volcanic changes brought about the extinction of the lake, when drainage systems broke eastwards through the DK Horst (defined by Stollhofen and Stanistreet, 2012). As early as the Ndutu Beds, rift valley subsidence and First Fault displacement provided depth potential, causing the Olduvai River to drain into the Olbalbal Depression (Fig. 1) through a proto-gorge (Hay, 1976). Previously westerly directed drainages (e.g. Stollhofen et al., 2008) were then replaced by the eastwardly directed Olduvai River fluvial system that continues to the present day. This is because by that time volcanoes directly adjacent to the basin were no longer active, so that the Olbalbal Depression was no longer continuously filled by volcanically sourced fans, as had been the case previously (Stollhofen and Stanistreet, 2012). As a result, the Ndutu and particularly the Naisiusiu Beds (Fig. 2) were deposited maximally within the developing gorge (Hay, 1976), so that ultimately the Naisiusiu deposits bypassed and

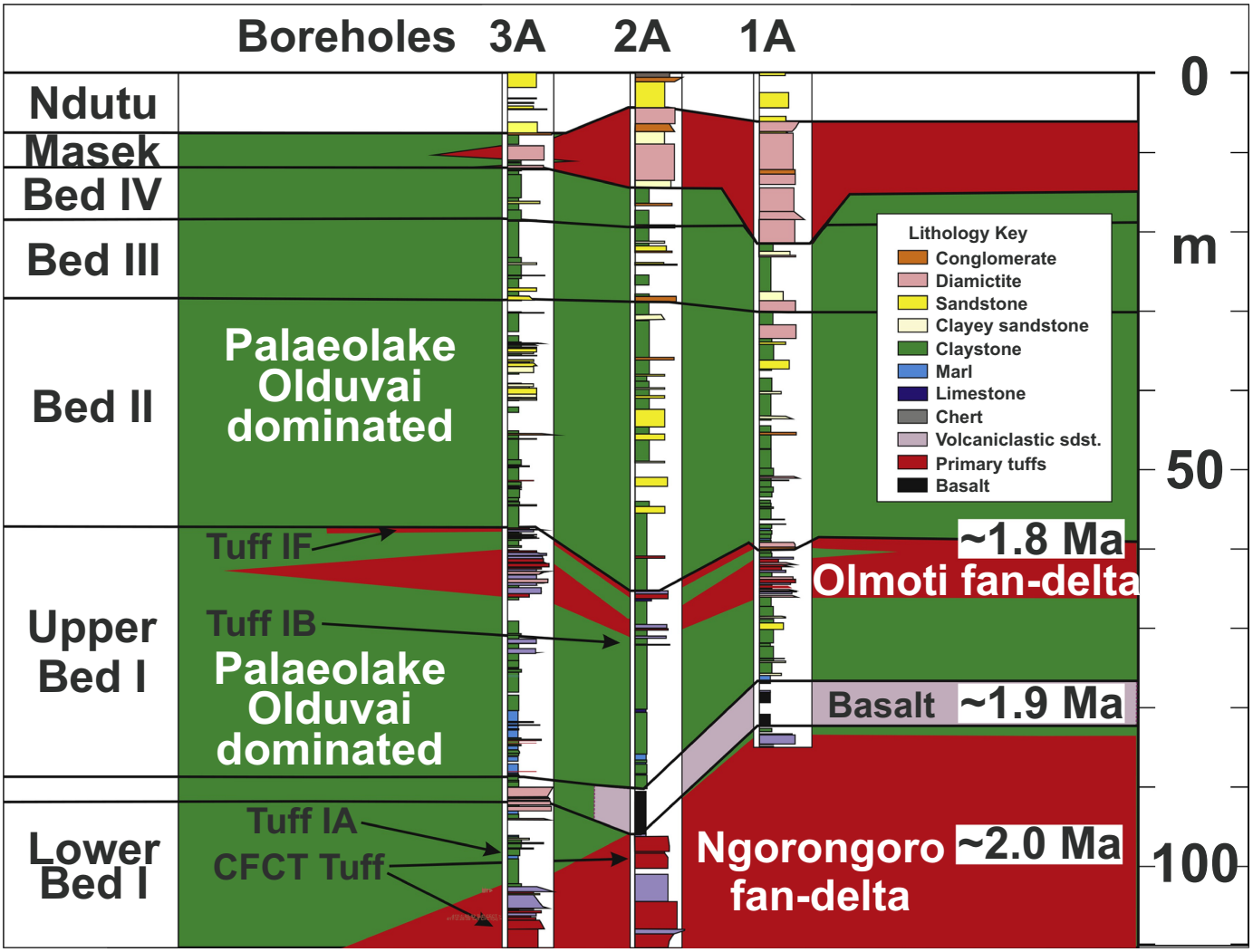

Fig. 3. Borehole cores 1A, 2A, 3A correlated, with the newly defined Ngorongoro and Naibor Soit Formations delineated as in Stanistreet et al., a this vol. Boreholes placed across tectonic grain and in position with respect to distance from Third Fault. Red = volcanically sourced fan-deltas. Green = lake dominated sequences, involving some fluvio-deltaics. Facies legend as for Fig. 6. (For interpretation of the references to colour in this figure legend, the reader is referred to the web version of this article.)

thus were not intersected at the drillsites. Therefore, the boreholes have captured almost the entire lake record within their extent.

Cores 1A, 2A and 3A were logged (Fig. 3) and sampled at set intervals for a variety of analyses (biomarkers, phytoliths, diatoms, ostracods, XRD, etc.), but the core intervals were also scanned for magnetic susceptibility, colour and natural gamma radiation, and subsequently analysed at high (1 cm) resolution by an XRF core scanner. The aim was to measure and stratigraphically extend the record of lake palaeosalinity proxies, originally identified by Hay and Kyser (2001), Berry (2012) and Deocampo et al. (2017) in outcrops from Bed I Tuff IA to lowermost Bed II (c. 1.78 Ma to 1.92 Ma) at Loc. 80 (Richard Hay Cliff or RHC) (Fig. 1) in the western Olduvai Basin. Our contribution significantly extends and refines the Olduvai palaeoclimatic/palaeosalinity record upwards to include the entire Beds I, II, III, IV and the Masek record (c. 0.5–2.0 Ma).

2. Present and past Olduvai climate and Ngorongoro Volcanic Highlands rain shadow effects

Olduvai Gorge is cut into the southeastern edge of the Serengeti Plain and presently experiences semi-arid climatic conditions associated with the development of savannah grasslands, with copses of and scattered acacia trees, associated with scrub. A weather station maintained at the Olduvai Research Camp (1966–1973, Hay, 1976) observed annual rainfall to vary from 27.6 cm to 105.2 cm per year (mean 57 cm), with maximum rainfall December to May, and largely dry June to August. Temperatures at the Olduvai Research Camp varied from 12 °C to 33 °C (1972/1973, Hay, 1976). The nearest currently operating weather stations recognised by the World Meteorological Organisation at Arusha and Mwanza register far higher mean annual precipitation (86 and 101 cm per year, respectively), but are both distant (150 and 280 km, respectively) and in very different geographical settings. The former sits to the east of the Ngorongoro Volcanic Highlands, the latter on the shore of Lake Victoria. The lower precipitation measured at Olduvai demonstrates the local rain shadow effect of the Ngorongoro Volcanic Highlands, as detailed later. At Olduvai wind blows most of the time, with prevailing winds from easterly quadrants (Hay, 1976 records an average velocity of 12.4 kph), although at times the Olduvai climate is affected by conditions from the west associated with Lake Victoria.

The palaeoclimate of East Africa has been overviewed for the study of the Lake Challa borehole cores (Verschuren et al., 2009; Moernaut et al., 2010), c. 500 km to the east of Olduvai. During July the Intertropical Convergence Zone (ITCZ) lies to the north of Tanzania, when the country is under the influence of the Indian Ocean, lying to the east of the Congo Air Boundary (Moernaut et al. (2010). The ITCZ then migrates southwards and lies to the south of Tanzania during January (Verschuren et al., 2009; Moernaut et al., 2010), when the Indian Ocean still dominates climatic effects. Biannual passage of peak insolation, generating maximum convective activity, causes two main rain modes, with the southeasterly monsoon bringing “long” rains March to mid-May and northeasterly monsoon bringing “short” rains during late October to December (Moernaut et al., 2010). During the last 24 kyr, Verschuren et al. (2009) record that the relative rain effects of the northeasterly and southeasterly monsoons vary with time, with the northeasterly monsoon dominant at 1 ka and 23 ka, and the southeasterly monsoon dominant at 11 ka. At intervening times, 7 ka and 18 ka, monsoonal influence is more symmetric and weaker.

The influence of the Indian Ocean on Lake Challa is however more straightforward than that on Olduvai Gorge. This is because the latter is situated 470 km from the Indian Ocean and to the east of the Ngorongoro Volcanic Highlands (NVH), which casts a pronounced rain shadow effect over the eastern Serengeti Plain in Tanzania, including Olduvai. According to known ages of NVH volcanoes their topography would have been rather similar during the Pleistocene, causing a rain shadow effect to the west (Peters and Blumenschine, 1995; Stollhofen et al., 2008; Mollel and Swisher III, 2012). The effect of this should be to enhance the contrast between orbitally induced wetter and drier phases at Olduvai, related to monsoonal strength. The height of the climatic barrier provides a pronounced threshold that would have been more easily crossed during times of enhanced monsoonal strength. At times of weaker monsoonal strength, aridity in the Olduvai area would have been exaggerated by the rain shadow effect. A further complicating factor on orbitally forced climatic variation at Olduvai therefore is that the NVH barrier would have extended further northwards with time through the Pleistocene. At the time of the earliest lake deposits recorded at the base of Borehole 2A (~2.4 Ma), only the extinct Lemagrut and Sadiman Volcanoes stood to the south-southeast of the Olduvai Basin. The evolution of Ngorongoro Volcano (~2.2 Ma to 2.0 Ma) would then have blocked the southeastern direction during the deposition of the Ngorongoro Formation (Fig. 3), after which Olmoti Volcano would have developed to the east of the basin during deposition of Bed I (~1.85 to 1.80 Ma). Subsequent volcanoes, Loolmalasin and Empagai (during deposition of Beds II, III, and IV, Mollel and Swisher III, 2012; Greenwood, 2014) sheltered the northeastern quadrant, whereas even younger volcanoes eventually developed to the north-northeast, completing the climatic barrier. A likely result would have been that the effects of southeasterly monsoonal winds were ameliorated throughout the deposition of the Olduvai Beds and that northeasterly monsoonal winds would have affected the Olduvai area more pronouncedly up until at least ~1.3 Ma. The only direct information on past wind directions at Olduvai is that from adhesion ripples in the Tuff IF unit (c. 1.8 Ma) of Bed I, indicating northeasterly winds (Stollhofen et al., 2008) and dune asymmetries and dune trails of the Holocene Namorod tephra, recording prevailing northeasterly and easterly winds (Hay, 1976).

3. Previous geochemical palaeosalinity proxy analysis from outcrop samples

To date Olduvai palaeoclimatic proxy analysis from outcrop has concentrated exclusively on Bed I and lowermost Bed II claystone-dominated sequences (Hay and Kyser, 2001; Ashley, 2007; Deino, 2012; Berry, 2012; Magill et al., 2013; Deocampo et al., 2017) mostly as they are exposed at Richard Hay Cliff (RHC, Loc. 80) (Fig. 1), as defined by Leakey (1971) and Hay (1976). Berry (2012) applied claystone whole-rock geochemical analyses of element oxides and element oxide ratios Al_2O_3/MgO, and TiO_2 values as palaeosalinity proxies, whereas Deocampo et al. (2017), using the same dataset, applied exclusively Al_2O_3/MgO ratios. Berry (2012) and Deocampo et al. (2017) apply the Al_2O_3/MgO ratio as a palaeosalinity indicator on the basis that high magnesium concentrations represent times when clays neoformed or were alteration products in the lake, preferentially developed during drier, more saline-alkaline periods. High aluminium concentrations on the other hand were argued to represent wetter periods when clays, formed in the lake catchment area, were transported directly as detritus into the lake. The principle is that periods dominated by detrital supply are rich in Al_2O_3 (present in K-feldspar, illite and Al-rich dioctahedral smectites) and TiO_2 (present in illite, and detrital Ti-oxides) (Hay and Kyser, 2001), while periods dominated by authigenic clay supply are enriched in MgO (particularly in Mg-rich trioctahedral smectites) (Hay and Kyser, 2001; Deocampo et al., 2017).

Deocampo et al. (2017) compared their Al_2O_3/MgO ratio proxy variation to stable carbon isotopic variation of leaf lipids in Olduvai Gorge clays (Magill et al., 2013), blown terrigenous sediment flux to the Arabian and the Mediterranean Seas, insolation curves for the northern Indian Ocean monsoon at Ngorongoro Crater, and modelled precession and eccentricity factors following Laskar et al. (2004). It was reasoned that magnesium uptake into authigenic clays (Jones, 1986; Webster and Jones, 1994; Calvo et al., 1999; Hay and Kyser, 2001), enhanced by reaction with lake water silica, a lower depositional rate, higher salinity, and higher pH, would mean that low Al_2O_3/MgO ratios would

register drier, more evaporative lake conditions. On the other hand, a high Al_2O_3/MgO ratio was hypothesized as indicative of lake "freshening" under wetter climatic conditions. Deocampo et al. (2017) identified between 1.82 Ma and 1.92 Ma six wetter phases and intervening drier phases, based upon the Al_2O_3/MgO ratio variation, that traced precessional climatic forcing. Between 1.855 Ma and 1.875 Ma, Colcord et al. (2018, 2019) confirmed the validity of two of these six wetter/drier cycles, that they named D1, W1, D2, W2, etc., using biomarker evidence. Consequently, we apply the Al_2O_3/MgO ratio as a palaeosalinity/palaeoclimatic proxy in this paper. However, palaeosalinity and palaeoclimatic variations are not the only control on magnesium input into a palaeolake. Absolute values of magnesium concentrations on the broader scale will relate to source rock type. This will inevitably vary in any basin where a variety of volcanic products are produced at different times. Magnesium availability in source rocks will achieve a maximum when basaltic magmatism dominates the source terrain (Stanistreet et al., this volume a,b); and during rhyolitic magmatism magnesium will be much less available. Because volcanic geochemistry varies over long periods at Olduvai (e.g., volcanoes typically last ~200 kyr in the NVH, Mollel and Swisher III, 2012), palaeoclimatic variation will be superposed on such low frequency geochemical shifts. It was therefore necessary to investigate source terrain aspects relating to magnesium and other element (e.g. titanium) concentrations to evaluate its significance.

Titanium is eroded from source rocks surrounding a basin (Jones, 1984; Cohen, 2003; Berry, 2012), particularly from basaltic and intermediate igneous rocks (Force, 1976) such as those that abut Palaeolake Olduvai. Titanium input is particularly enhanced during wet climatic phases when chemical weathering, erosion and transport rates are maximised. Thus, Ti can be used as a proxy for detrital siliciclastic flux, which will partially dilute the Mg supply, leading to an increased Ti concentration. In periods without substantial Mg or carbonate enrichment, a correlation between Ti supply rate and Ti concentration in the sediment is no longer inevitable, as there needs not be a Ti-poor component to be diluted. Analysis of stratigraphic variations in Ti count values (typically enriched in clay minerals and silt-sized oxides), Zr (typically enriched only in the silt size fraction), and Rb (enriched in clay minerals) suggests that Ti is predominantly present in silt sized detrital grains. This would mean that Ti enrichment indicates coarser and more energetic sediment delivery during wet phases, diluting finer Ti-poor sediments.

Accordingly, Berry (2012) found that the Al_2O_3/MgO and TiO_2 proxies she applied co-varied cyclically when plotted against stratigraphic depth, and that cyclic periods were forced by both obliquity and precessional climatic oscillations as defined by Milankovitch (1941, 1998). However, because there was less spread of data, the Al_2O_3/MgO ratio expressed the cyclic variation best and as a result this was the proxy applied from the same dataset by Deocampo et al. (2017). One of the causes of data spread affecting proxy values deriving from outcrop samples is the variable weathering that rocks will have experienced on exposure to the atmosphere. However, XRF measurements based on borehole core samples have the potential to reduce such spread and to provide a clearer palaeoclimatic proxy signal.

4. Methods

Boreholes were drilled using an Atlas Copco CS 14 Diamond Core Drill Rig, using HQ3 surface set core bits (3.782″ × 2.400″) and, as far as possible, exclusively water as drilling fluid. All depth values are recorded as total depths in metres below the surface. Drilling employed the HQ3 triple tube method, whereby cores were collected and sealed in polycarbonate liners. After halving the cores at the LacCore facility at the Twin Cities campus of the University of Minnesota, the two halves were designated as either Archive (A) or Working (W) half, the latter used for sampling purposes. The Archive half of the core was logged at mm to cm scale and subsequently sent to the Duluth Campus of the University of Minnesota, where they were XRF scanned using an ITRAX Core Scanner made by Cox Analytical Systems. The scanner was configured as follows: kV = 30; mA = 15; stepsize 10 mm; X-Radiograph kV = 60; X-Radiograph mA = 30; X-Radiograph Step Size = 0.02 cm. The chromium (Cr) tube was used and the dwell time was 15 s per sample interval. The core face was prepared flat, free of extraneous materials, and covered by Chemplex Ultra-Polyester, 1.5 μm thick plastic film. The scan results were provided as Excel spreadsheets, and verified, quality-assured and depth corrected by the Duluth laboratory. All data points related to facies that are not either claystones or sandy claystones were excluded from the following analyses and graphs, to minimize grain-size and other facies effects on geochemistry. Correlation between cored strata (Fig. 3) is based on sequence stratigraphic (c.f. Stanistreet, 2012; Stanistreet et al., 2018a, 2018b) and tephrostratigraphic principles, the latter based on the occurrence of unique textures, juvenile mineral assemblages, glass and single grain compositions. Microprobe analyses of these grains provided geochemical "fingerprints" of tuff marker horizons (McHenry et al., this volume).

Our palaeosalinity and palaeoclimatic proxy analyses apply the same elements and element ratios identified by Berry (2012) and Deocampo et al. (2017) as Palaeolake Olduvai salinity proxies. While Berry (2012) measured element concentrations, reported as oxides, using whole-rock X-Ray fluorescence spectroscopy of claystone samples, the XRF scanning method applied to the OGCP cores here, reported x-ray counts. Measured in air, Mg is below the detection limit in many samples. The Al/Mg counts ratio and Ti counts were plotted, but it was found that because Mg counts were frequently registered as zero values, it was more convenient to plot the Mg/Al counts ratio to derive graphable values. This means that the resulting ratio variation is a mirror image of the Al_2O_3/MgO variation used by Berry (2012) and Deocampo et al. (2017).

5. Results

We use the raw count data for 12,372 individual XRF analyses, collected every 1 cm for the claystone and sandy claystone intervals of Cores 2A and 3A, to examine geochemically discernible cyclicity, with a focus on Al, Mg, and Ti. Individual data points (either single elements or ratios) are plotted against depth in core in Fig. 4 (and later figures), showing changes in composition with depth. Fe is additionally used (Fig. 5), to show the relationship between clay compositions and the Bed I basaltic lavas.

Primary age control is provided by the identification of specific marker tuffs within the cores, which have previously been dated from outcrop sampling. In particular, the Coarse Feldspar Crystal Tuff (CFCT, 2.015 ± 0.006 Ma, Deino, 2012), Tuff IB (1.848 ± 0.003 Ma Deino, 2012), and Tuff IF (1.803 ± 0.002 Ma, Deino, 2012) are all identified in Core 2A (see McHenry et al., this volume; Stanistreet et al., this volume a, b), and provide the framework for an age model for Olduvai Bed I within the cores. As discussed in detail later, these correlations and dates provide chronological constraints on the cyclicity described.

Fig. 4 shows Mg and Al counts measured from Bed I and Bed II claystones and sandy claystones from Cores 2A and 3A. Firstly, the plot registers an overall positive magnesium anomaly (c. 100–300 cps), outstanding with respect to the background to trace values (50–100 cps) recorded in the remainder of the Olduvai Beds. The Mg anomaly is observed in correlative sections of both cores: in Core 2A below 65 m; and in Core 3A between 55 m and 98 m. This anomaly encompasses Lower Bed II, Upper Bed I and the upper half of the Lower Bed I claystones. Al values are mostly <1000 counts for most of Lower Bed I (upper part) to Upper Bed I (lower part) claystones, but show elevated values in the sub Tuff IA part of Lower Bed I in Core 3A and an overall increase (<1800 cps) above Tuff IF. Secondly, repeated magnesium count maxima (up to 330 cps) are nested particularly within the overall positive anomaly. Al values vary cyclically at metre intervals

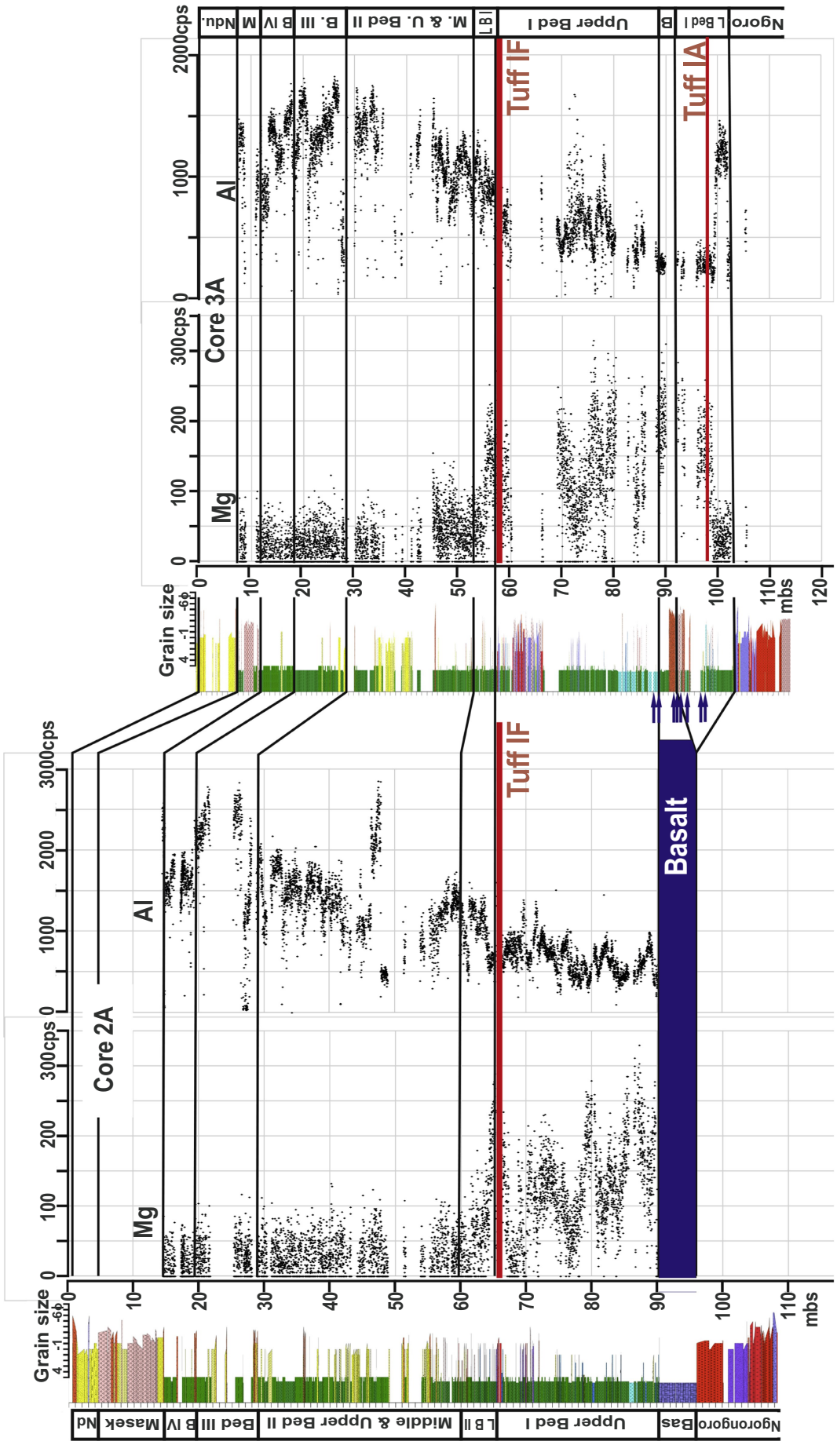

Fig. 4. Mg and Al counts per second (cps) in Beds I and II claystone and sandy claystone facies of Cores 2A and 3A (see Fig. 2 for stratigraphic position of section). Mg-rich portions of: Core 2A are below 65 m; and of Core 3A are between 55 mbs and 98 mbs, this is referred to as the "Bed I Mg anomaly". Blue arrows indicate positions of mafic tuffs. Note that the lacustrine portion of Lower Bed I is missing from Core 2A, where its position is represented by a major unconformity directly below the basalt. Note that Mg-count cycles tend to mirror those of Al-counts. Facies legend as for Fig. 6. Grain size is given in φ units, whereby -1φ is the sand/gravel boundary and 4φ is the silt/sand boundary. (For interpretation of the references to colour in this figure legend, the reader is referred to the web version of this article.)

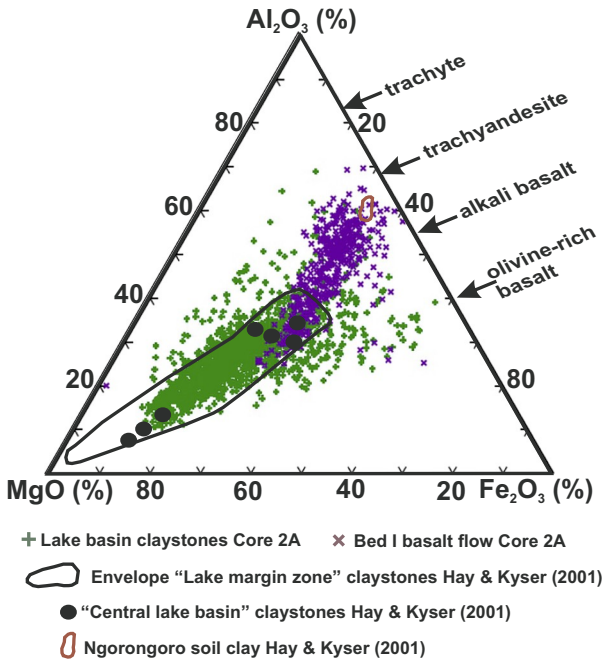

Fig. 5. Core 2A XRF scan results show that the Bed I lake claystone geochemistry (green crosses and "lake margin zone" claystone envelope of Hay and Kyser, 2001) of the Bed I Basalt to Tuff IB interval is dominated by an alkali basalt source, typical of continental rift settings, but the Bed I basalt (purple crosses) itself plots between alkali basalt and trachyandesite compositions. This is more in line with the results of Habermann et al. (2016b) who classify the Bed I lava flows and associated tuffs of the eastern gorge as basalts and trachybasalts, the latter rock type intermediate between basalts and basaltic trachyandesite. This might indicate that the major proportion of the lake clays are neoformed from weathering of mafic tuffs and basalt lavas associated with Ngorongoro bimodal volcanism, well comparable with compositions of Ngorongoro soil clays (Hay and Kyser, 2001) outlined in red. (For interpretation of the references to colour in this figure legend, the reader is referred to the web version of this article.)

throughout both cores within ranges of approximately +/− 700 counts. It should be noted that Mg and Al are broadly antipathetic. Cyclic variation of Mg counts thus tends to mirror those of Al-counts.

Fig. 6 shows a comparison between: magnesium and aluminium concentrations, introduced by Berry (2012) and Deocampo et al. (2017) and expressed here as the Mg counts/Al counts ratio; and another element concentration applied to Olduvai by Berry (2012), that of titanium. Cycles of variation in titanium content were found to mirror those of the Mg counts/Al counts ratio. In terms of Cores 2A and 3A as a whole, titanium concentration proved to be the most reliable overall, registering well in all Beds I to IV and Masek Beds, rather than just Bed I, as was the case with magnesium abundance.

We will now evaluate causes of the Bed I magnesium anomaly, sources affecting lake clay geochemistries and in particular the origin and timing of cyclic element counts and count ratios.

6. Discussion

6.1. The Bed I magnesium anomaly and primary carbonate layers

Berry (2012) and Deocampo et al. (2017) apply the Al_2O_3/MgO ratio as a palaeosalinity indicator on the basis that high relative values of magnesium concentration represent times when clays neoformed or were alteration products in the lake, preferentially developed during drier, more saline-alkaline periods. High aluminium concentrations on the other hand were argued to represent wetter periods when clays, formed in the lake hinterland, were transported directly and detritally into the lake. Deocampo et al. (2017) further showed that the Al_2O_3/MgO ratio co-varied with changes in biomarker analyses of Magill et al. (2013) that were also interpreted to indicate palaeoclimatic change. As mentioned earlier, the cyclic variation of the Al_2O_3/MgO ratio only records adequately during the magnesium anomaly within Bed I, when the influx of Mg during basaltic magmatism was sufficient to provide a palaeoclimatic register.

It is no coincidence that the first primary carbonate units (dolmicrite, limestone, marl) logged in Core 3A (median depths (mbs = metres below surface) at 99.0, 98.7, 98.1, 96.2, 94.2, 94.0, 93.8, 93.3, 92.6, 92.4, 92.1, 91.5, 90.8, 76.1, 75.9, 66.2 m) follow immediately after initiation of the magnesium anomaly (Fig. 4; see also Stanistreet et al., this volume b, their Fig. 5). Indeed, primary limestone and dolomite layers deposited in Palaeolake Olduvai were formed exclusively during the stratigraphic extent of the magnesium anomaly. Calcium as well as magnesium inputs were enhanced during this part of Bed I and Lower Bed II, and high Mg/Ca ratios in the lake waters would have promoted dolomite deposition and/or dolomitization of pre-existing limestone. However, the predominance of primary dolomite deposition is indicated by the fact that carbonate nodules, associated with pedogenically overprinted lake claystones, show no signs of secondary dolomitization (Bennett et al., 2012; Rushworth, 2012; Stanistreet et al., this volume b).

6.2. Basaltic volcanic source affecting Bed I and Lower Bed II lake clay geochemistries

Absolute magnesium abundance in a sedimentary basin is controlled not by climate, but by source terrain chemistry. The magnesium anomaly just described is caused by a phase of basaltic volcanism within the Olduvai Basin, and this requires more consideration. Fig. 5 is an AFM triangular diagram, which format is based upon the pioneering outcrop work of Hay and Kyser (2001), that relates Bed I (Basalt to Tuff IB interval) claystone geochemistries of Core 2A directly to analyses of the Bed I Basalt, representing a parental magmatic source. Pre-Tuff IB geochemistries were chosen exclusively because after this eruptive event trachytic compositions related to Olmoti Volcano added to the magmatic sources of the clays. To generate Fig. 5, Al, Fe and Mg X-ray counts in concentration units needed to be converted to oxide values. This has been accomplished by assuming that basaltic layers scanned have the composition (Krauskopf, 1995) of average basalt (Table 1), forming the basis for this calibration.

Hay and Kyser (2001) deduced that clays of Bed I, compositions of which were enveloped by a black outline in Fig. 5, are derived from weathering of alkali basalts. Another composition for comparison was that of "Ngorongoro soil clays" (Hay and Kyser, 2001), neoformed from weathering of mafic tuffs and basalt lavas of the NVH and marked by a red outline in Fig. 5. Our XRF scan results of Core 2A lacustrine claystones and Bed I basalt lava are graphed as individual points in Fig. 5. Most of the claystones (green crosses), including those from offshore settings, plot within a field that corresponds to the "Lake margin claystones" envelope of Hay and Kyser (2001), but do not trend as far towards the MgO extreme as the "Central lake basin" claystones they document. The correspondence between the two datasets supports the validity of the oxide calibration outlined above. Basalt analyses (shown as purple crosses) from Core 2A concentrate at one point on the diagram, commensurate with a trachyandesitic to alkali basaltic composition. A trend towards the MgO corner of the AFM triangle overlaps with the maximum concentration of claystone compositions, and this might represent initial in situ and early diagenetic alteration of the basalt prior to erosion and transportation. A smaller number of outliers trend towards the Fe_2O_3 corner of the AFM triangle. This might correspond to reddened, weathered portions of the basalt, noted in some outcrop equivalents, and generally associated with weathering of pahoehoe flows and other flow top features (e.g., Habermann et al., 2016b).

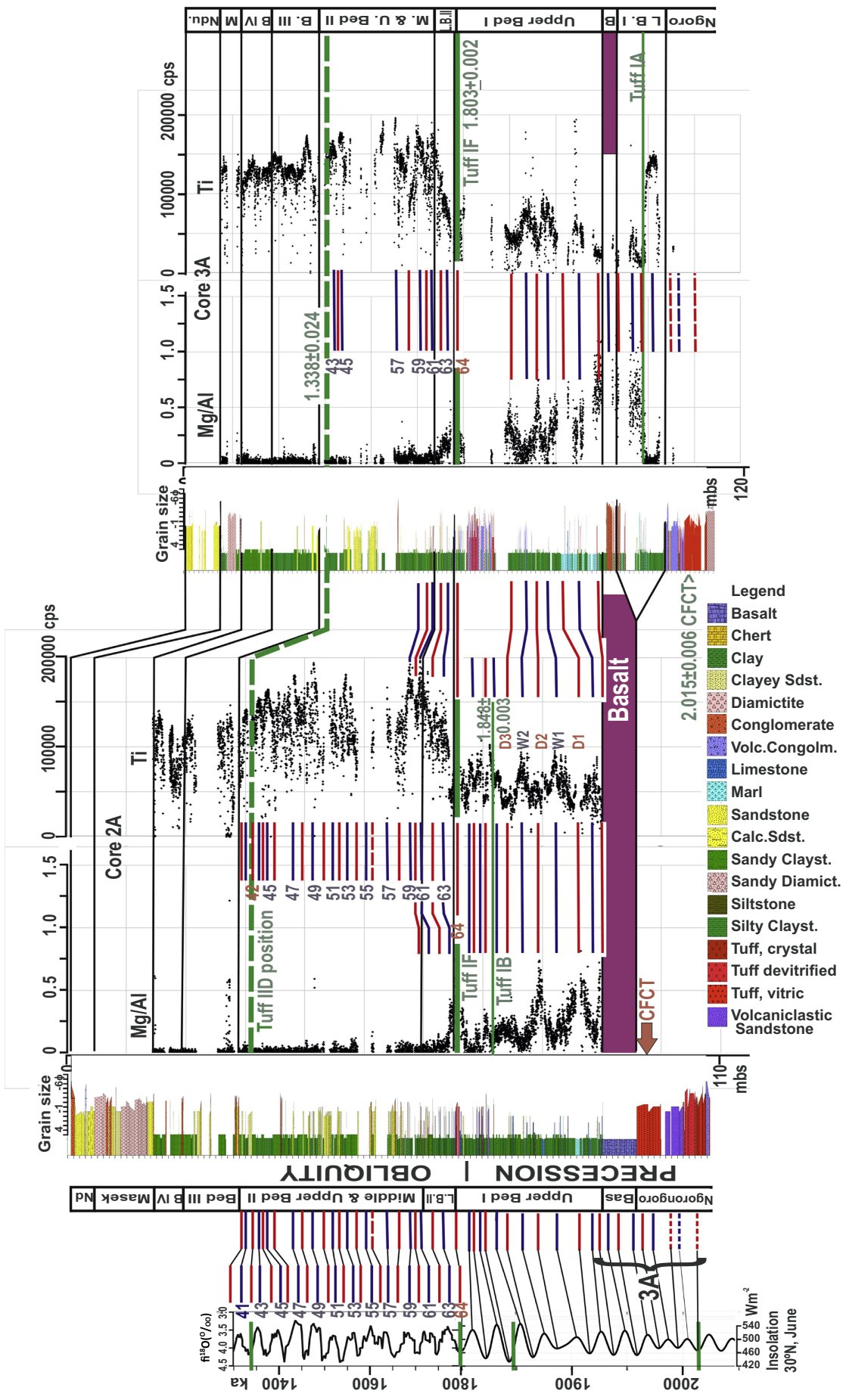

Fig. 6. Palaeosalinity and palaeoclimatic proxies Mg/Al, and Ti (cps = counts per second) plotted for Beds I, II, III, and IV, Cores 2A and 3A. For the latter lacustrine Masek Beds are also shown. Note that Lower Bed I claystones are missing from Borehole 2A due to a sub-Basalt unconformity. Purple unit = basalt, only present in Core 2A, but scoria-rich sediment layers mark basalt position in Core 3A. Green lines highlight positions and correlations between marker tuffs, identified geochemically by McHenry et al., this volume. Indicated radiometric dates are based on Deino (2012: CFCT, Tuff IB, Tuff IF) and Domingo-Rodriguez et al. (2013: Tuff IID). CFCT = Coarse Feldspar Crystal Tuff of Hay (1976). Red lines mark drier phases and blue lines mark wetter phases based on geochemical proxies. Red D numbers and blue W numbers = Wet and Dry phases of Colcord et al., 2018, 2019 this volume and Shilling et al., 2019). Red dashed lines (indicating subaerial volcanics) and blue dashed lines (indicating transgressive claystones) indicate dry and wet phases based upon sedimentological criteria rather than elemental count variation. Recognised Wetter and Drier phases are correlated to the modelled precessional (~23 kyr period) insolation record (Laskar et al., 2004) for Bed I. With reference to the obliquity (~41 kyr period) dominated marine isotope record, numbers of Marine Isotope Stages (MIS) (Lisiecki and Raymo, 2005) are allocated to relevant Bed II cycles. Facies legend is valid for all figures showing core. Grain size is given in φ units, whereby -1φ is sand/gravel boundary and 4φ is silt/sand boundary. (For interpretation of the references to colour in this figure legend, the reader is referred to the web version of this article.)

Table 1
Calibration factors used in converting Al, Fe and Mg counts to oxide values, based upon average determinations published by Krauskopf (1995).

	Count rate	Concentration wt%	Factor
Fe_2O_3	538,381	12.3	2.28E-05
MgO	114	7.5	6.57E-02
Al_2O_3	2268	15.9	7.00E-03

Fig. 5 suggests that the magnesian contents of the claystones of Upper Bed I are derived from Ngorongoro basaltic volcanic products. Thus, the overall abundance of Mg in Fig. 4 relates to a volcanic source, likely weathering of explosive volcanic products, because weathering is most effective in glass-rich, vesicular ash due to its highly reactive particle surfaces. The onset of the Mg anomaly maximum coincides with the successive effusions of the Bed I Basalt flows, but additionally and more significantly coincides with the deposition of three thin basalt scoria-rich layers (marking the correlative position of the Bed I basalt, Stanistreet et al., this volume a) and the deposition of five mafic tuff units, all of whose positions are indicated by the blue arrows adjacent to the log of Core 3A in Fig. 4. Core 3A shows that Mg input into the lake basin initiated prior to the Bed I basalt lava emplacement and even prior to Tuff IA. More specifically the onset of the Mg-anomaly can be located at exactly 99.4 mbs depth in Core 3A, about 98 cm below Tuff IA. The Mg anomaly onset is therefore located in the middle of a major claystone unit that marks a pronounced Bed I lake transgression just after the termination of major Ngorongoro acid to intermediate volcanism. The magnesium anomaly onset is marked by a pronounced colour change from olive green sandy claystones below to brown-olive claystones above. Additionally, there is a pedogenic layer of carbonate nodules marking the top of the underlying unit, which would suggest pronounced lake drying and/or emptying (Bennett et al., 2012; Rushworth, 2012; Stanistreet et al., this volume b) and an associated hiatus just prior to the magnesium anomaly. The Bed I basalt flows were emplaced within or even as a culmination of that basaltic effusive phase, more precisely as the basic end-phase of the bimodal (Habermann et al., 2016a, 2016b) volcanism of Ngorongoro Volcano, the cone of which is formed by rhyolitic/trachytic lavas and pyroclastics (Mollel and Swisher III, 2012). The basaltic phase represents the completion of the bimodality, with mafic magmas reaching the surface, resulting in the effusion and explosive eruption of basaltic melts to form the mafic tuffs and lava flows of Upper Bed I.

6.3. Palaeosalinity/palaeoclimatic changes proxied by Mg counts/Al counts ratio and Ti counts

Fig. 4 shows the benefits of data gathered from unweathered cores for geochemical proxies in the form of a well-developed cyclicity in both the Mg and Al count profiles of cores 2A and 3A. However, the Mg count profiles only show a clear cyclic record between 55 m to 100 m of both cores, when the basin was deepest, the lake most extensive, and when Mg counts are high enough for reliable measurement during the development of the magnesium anomaly. So, it was fortuitous that the analyses of Berry (2012) and Deocampo et al. (2017) were undertaken on this portion of the sequence, otherwise the potential of the Mg/Al ratio might not have been recognised.

Accordingly, Fig. 6 plots both the Mg/Al ratio and another proxy applied by Berry (2012), that of titanium. Cohen (2003) points out that titanium is eroded much more readily from bedrock sources during wetter climatic phases (blue lines in Fig. 6), in the same way as aluminium shown in Fig. 4. Indeed, titanium and aluminium should co-vary, because both are supplied within particulates eroded from catchment soils. In contrast during drier times (red lines in Fig. 6) titanium input is minimal. Abundance of titanium (cf. Jones, 1984) and its co-variant elements therefore serve as a proxy for wet/dry climatic cycles. Berry (2012) used TiO_2 as a climatic proxy, but we plot Ti counts in Fig. 6. She found that TiO_2 was co-variant with the Al_2O_3/MgO ratio, and accordingly Fig. 6 plots Mg/Al counts, as explained earlier, with the ratio variation mirroring that of Ti counts in terms of cyclicity. The interval in which both Mg/Al count ratio and Ti count cyclicities are most clear is that bracketed by the Bed I Basalt and Tuff IB, particularly in core 2A (Fig. 6).

Sedimentary indicators such as high total organic carbon (TOC) values (Shilling et al., 2019, this volume; Ferland et al., 2020 this volume), preservation of sub-millimetric (possibly annual) laminae, lack of wave reworking, and lack of rooting or burrowing (Colcord et al., 2018, 2019) indicate that Palaeolake Olduvai was deepest and probably commonly a thermally layered, meromictic lake body recorded in Core 2A below 72 mbs depth, the Bed I Basalt to Tuff IB interval that contains the Mg anomaly. Meromictic stratification of lake water would favour anoxic conditions on the lake bottom, suppressing biological activity and oxidation of organic matter at those times. Lake depth is not solely a function of palaeoclimate, but a combination of precipitation and tectonic subsidence, in the case of the Olduvai Basin due to syndepositional crustal stretching and extension (Stollhofen and Stanistreet, 2012). During Bed I, the resulting maximal accommodation space within the Olduvai Basin coincided with the basaltic magmatic phase, causing the magnesium anomaly. Therefore, basaltic magmatism, with its resulting magnesium anomaly, and basin deepening are both ultimately caused by crustal stretching, causing enhanced basin subsidence and opening crustal pathways for basaltic magma ascent (Shaw, 1980) at the same time.

Because Lower Bed I is entirely missing from Borehole 2A and the Bed I Basalt from Borehole 3A (although equivalent sedimentation can be recognised in the latter), Fig. 6 plots cycles of Mg, Al and Ti variance for Bed II and Upper Bed I in Core 2A and for Bed II, Upper and Lower Bed I, together with the interval representing the Bed I Basalt in Core 3A. The Mg/Al proxy is pronounced in Bed I because of high Mg values related to the dominantly basaltic effusives of the late Ngorongoro bimodal volcanic source discussed earlier. The Ti proxy is more abundant in Bed II because of the Ti-rich phases associated with basaltic volcanism at that time, speculated by Greenwood (2014) as possibly related to Loolmalasin Volcano, placed as just younger than Olmoti Volcano by Mollel and Swisher III (2012). Blue lines mark Ti maxima and Mg/Al minima as wetter climatic phases and red lines as the complementary drier phases. Because Mg counts are adequate in Bed I, both proxies are applied to that stratigraphic interval to determine climatic cycles, but because Mg counts are insufficient in Bed II, only the Ti proxy is used at that level.

6.4. Orbital control on proxy element count cyclicities in Beds I and II

To date palaeoclimatic proxy analysis has concentrated exclusively on Bed I and Lower Bed II claystone-dominated sequences (Hay and Kyser, 2001; Ashley, 2007; Stanistreet, 2012; Deino, 2012; Berry, 2012; Magill et al., 2013; Deocampo et al., 2017), mostly because they are well exposed at Richard Hay Cliff (RHC, Loc. 80) (Fig. 1), with tuff layers and their correlatives (McHenry, 2005, 2012) dated elsewhere in the Olduvai Basin (Deino, 2012) providing a reliable framework for the timing of cyclicities. In most cases previous authors detected cycles that were precessional with a period of ~23 kyr, but obliquity-related climate oscillations were also identified (e.g. Deocampo, 2004; Berry, 2012). In their initial biomarker analyses of Core 2A, Colcord et al. (2018, 2019) concentrated on TOC-rich portions of Core 2A, also contained in Upper Bed I, and also detected correlatory precessional variations. This cyclicity is now apparent in palaeosalinity/palaeoclimatic variation inferred from Ti (and related element) count variation within Upper Bed I of Core 2A, and such cycles can now be shown to extend down through the time of lava effusion of the Bed I Basalt unit, and further down throughout Lower Bed I. Fig. 6 shows 9½ wet/dry cycles between the Coarse Feldspar Crystal Tuff (CFCT) (Deino, 2012:

2.015 ± 0.006 Ma) and Tuff IF (Deino, 2012: 1.803 ± 0.002 Ma). The average sediment accretion rate during this interval is 48.9 m in 212 kyr or 0.23 mm/yr and the period of the cycles is ~22.3 kyr. Cyclic duration correlates to a precessional variation as indicated in the lower part of Fig. 6, encompassing on average 5.1 m of sequence each. This confirms and stratigraphically extends the precessional cyclicity recognised in the more stratigraphically limited ranges dealt with previously. Timewise, the correlated cycles are constrained by three $^{40}Ar/^{39}Ar$ dated marker tuffs, Tuff IF (Deino, 2012: 1.803 ± 0.002 Ma) at the top, Tuff IB (Deino, 2012: 1.848 ± 0.003 Ma) in the middle and the CFCT (Deino, 2012: 2.015 ± 0.006 Ma) at the base, all of which have been identified mineralogically and geochemically in Core 2A (McHenry et al., this volume).

Stanistreet (2012) additionally recognised the sedimentary register of a frequency lower than precessional in the palaeoclimatic transgressive/regressive events affecting uppermost Bed I and Lower to Middle Bed II of the margin around Palaeolake Olduvai. This he correlated to the $\delta^{18}O$ Marine Isotope Stage record (Shackleton et al., 1995) and the monsoonal aeolian dust record in the Arabian Sea (Bloemendal and deMenocal, 1989; deMenocal and Bloemendal, 1995), corresponding to the Milankovitch obliquity record. Milankovitch (1941, 1998) himself considered that such ~41 kyr obliquity cycles would have the greatest effect on climate, and in oceanic records it proved to be the case between one and three million years as recorded by $\delta^{18}O$ ($^{o}/_{oo}$) variation. Lisiecki and Raymo (2005) attached MIS Stage nomenclature to variation of benthic $\delta^{18}O$ values measured from the Pliocene-Pleistocene and Holocene of multiple deep oceanic cores worldwide. During the time interval studied in their paper it was the ~41 kyr obliquity cycle that forced temperature change in their core record. Stanistreet (2012) recognised such obliquity effects, controlling the generation of erosional sequence boundaries within the sedimentary succession of Palaeolake Olduvai's margin and hinterland, demonstrable at outcrop. However, the OGCP boreholes were drilled into the depocentre of Palaeolake Olduvai, where more expanded, and less erosionally affected sequences were deposited. This allows such lower frequency climatic signals to be more completely preserved.

Accordingly, the sediment thickness of Bed II in Borehole 2A is 27.2 m between Tuff IF (1.803 ± 0.002; Deino, 2012) and the correlatory position of Tuff IID (1.338 ± 0.024; Domínguez-Rodrigo et al., 2013) during 465 kyr, amounting to an average accretion rate of ~0.058 mm/yr, almost a fifth of the rate reconstructed for Bed I. This is too slow to identify the precessional periods recognised in the latter. However, there are 11.5 wet/dry cycles recognised in this 465 kyr interval, suggesting 40.4 kyr per cycle, each cycle occupying on average about 2.4 m of sequence. These accord with the obliquity cycles already recognised by Stanistreet (2012) in Lower Bed II, rather than the precessional cycles recognised lower down. This does not mean to say, however that the obliquity effect will not register during Bed I and Lower Bed II, rather that the effects will superpose, as recognised by Berry (2012). Fig. 6 shows the record of these wet-dry intervals in Bed II, as archived in the Ti proxy, and ties these to Marine Isotope Stages (MIS) 40–64. The rain shadow effect of the adjacent Ngorongoro Volcanic Highlands would have accentuated the difference between arid and humid intervals during this period, as this barrier would have limited the incursion of weaker Indian Ocean derived monsoons (during arid periods) but had less effect on more powerful monsoonal systems (during humid periods).

Astronomically forced palaeoclimatic cycles have been identified in this study from Beds I and II of the Olduvai sequence, however the process has been extended to Beds III, IV, and the Masek Beds (Figs. 4 and 6). The completion of that analysis awaits the finalisation of ongoing palaeomagnetic and radiometric dating of the cores.

6.5. The Tuff IF hyper-arid phase

A key interval in the climatic record is the meeting between the two dominating precessional and obliquity-forced cyclic records, at a time when a terminal eruption from Olmoti Volcano laid down Tuff IF. Fig. 6 shows that climatically this time is marked by a coincidence of a minimum in the precessional variation at the top of Bed I and an obliquity minimum at the base of Bed II. That dry phase correlates with the glacial phase Marine Isotope Stage MIS 64 located by Lisiecki and Raymo (2005). In the Olduvai Basin, this period has previously been recognised as an especially dry phase as recorded by Stanistreet (2012), on the basis of Stollhofen et al. (2008) and Bamford et al. (2008). The latter found that even at RHC/Loc. 80 (Fig. 1), within a deeper water lacustrine claystone outcrop succession there (Fig. 7), Tuff IF pyroclastic surges (facies described in Stollhofen et al., 2008) were subaerially deposited in contrast with all the other, lacustrine waterlain, thin Olmoti Tuffs IB, ID, IE and Ng'eju at this site (McHenry, 2005).

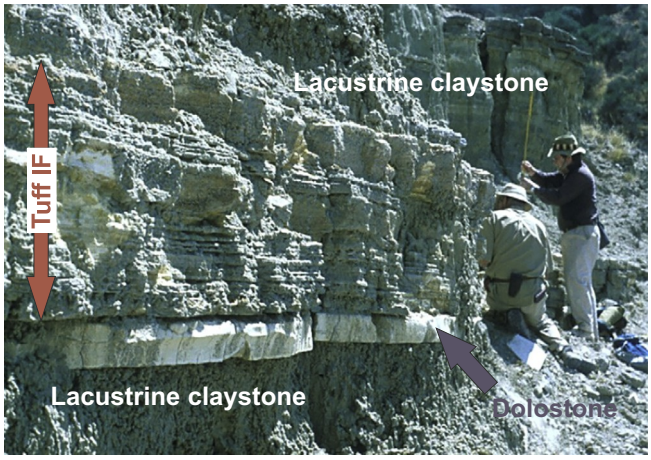

Fig. 7. Tuff IF exposed at Richard Hay Cliff (Loc. 80); see Fig. 2 for stratigraphic position of photo. Richard Hay and IGS are remeasuring the Tuff IF unit. For detailed measurements and facies descriptions/interpretations see Stollhofen et al. (2008). Note that the base of Tuff IF sits upon a slightly incised erosion surface. In this locality a thin claystone is preserved between the dolostone layer and IF, as is the case in Core 3A, but in Core 2A the surface cuts down into the underlying carbonate. Stratigraphic equivalence of this outcrop shown by double ended vertical black arrow in Fig. 8.

The presence of vesiculated surges within the Tuff IF marker unit at RHC showed that it was emplaced subaerially, sandwiched by thin shallow water wave-reworked tuffs at the top and bottom (Stollhofen et al., 2008). That determination was made on the upthrown side (footwall) of Fifth Fault (RHC), whereas the OGCP boreholes were all sited on the downthrown side (hangingwall) of Fifth Fault further into the basin depocentre towards the deepest part of the lake. Cores 2A, 3A and 3B now revealed that the vesiculated surge facies of Tuff IF at RHC was also developed even in this deepest part of the lake. The implication was that the lake basin was almost empty at that time. Palaeoclimatically this confirms climatic controls rather than any other mechanism, such as volcanically induced "mock aridity" (c.f. Harris and Van Couvering, 1995).

6.6. Tuff IA aridity

Another phase of aridity is recorded at the time of the emplacement of Tuff IA. Tuff IA is rarely preserved as a "primary", non-reworked tuff. In the cores, Tuff IA is preserved as a ~15 cm thick layer of volcaniclastic debris flow facies. At Locality 66e (Fig. 1), as is demonstrable in most of its western Olduvai Basin outcrop exposures, Habermann et al., 2016a recorded the unit as a 10–20 cm thick fluvially reworked tuff layer. Only at Locality 53 (Fig. 1) have primary (non-reworked) tuff facies yet been identified within the unit. Fig. 8 shows the top of the Ngorongoro Volcanics Formation (Stanistreet et al., this volume a). The last major eruption to occur in this unit was the CFCT (Coarse Feldspar

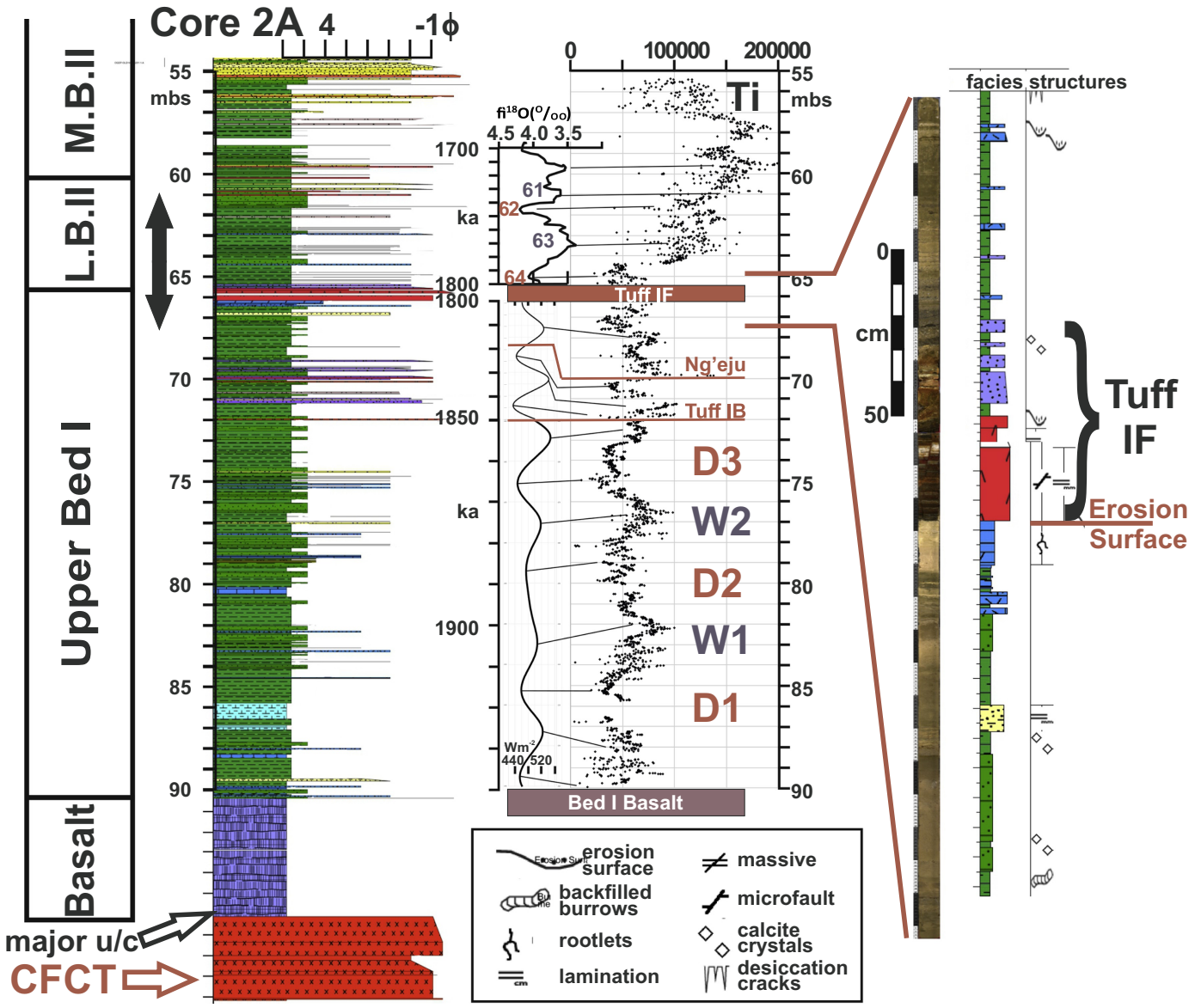

Fig. 8. Detailed placement of Tuff IF (Core 2A) into the climatic changes of Upper Bed I and Lower Bed II proxied by variation in titanium input into the basin. Tuff IF was laid down during a phase of hyper-aridity (Stollhofen et al., 2008; Bamford et al., 2008; Stanistreet, 2012) when the lake was almost empty. The hyper-aridity was due to the coincidence of an obliquity dry spell (MIS 64, see marine isotope variation above Tuff IF) on a precessional dry period (see insolation variation below Tuff IF). Double ended black vertical arrow indicates stratigraphic equivalent of Fig. 7. Red D1, D2, D3 and blue W1, W2, W3 refer to dry and wet phases defined by biomarkers (Colcord et al., 2018, 2019; Shilling et al., 2019, this volume). Facies legend as for Fig. 6. (For interpretation of the references to colour in this figure legend, the reader is referred to the web version of this article.)

Crystal Tuff = Tuff NgQ) represented by an unwelded pyroclastic flow facies in Core 2A. Progressing upwards the abandoned fan surface was covered by transgressive lake claystone deposits, associated with pronounced (see also Fig. 6) wetter climate. Initially, the claystones are uniform, representing massive fine-grained deep lake facies, at drilling depths between 100 and 102 mbs. As the cycle completed, the palaeoclimate progressed into the precessionally forced drier phase (Fig. 9). Accordingly, more varied sedimentary structures are present within that interval, notably many erosion surfaces and desiccation crack horizons, together with burrows and rootlet bioturbation (Fig. 9). Sandy and gravelly diamictite layers are also present, marking lake drying phases within the basinal depocentre (see also Stanistreet et al., this volume b). At about the middle of the drier part of the cycle, Tuff IA was erupted and deposited onto a surface on which pronouncedly deep desiccation cracks had previously developed. A crack that has fortunately been intersected by the borehole extends as deeply as 23 cm below the horizon (Fig. 9). The clay unit above and below Tuff IA is therefore particularly effective in showing the sedimentary structure variation typically developed during a complete Bed I precessional climate cycle in the lake depocentre.

7. Further implications of the identification of wet/dry cycles in Beds I and II

The recognition of climatically forced cycles within large parts of the lake sediment profiles also allows more precise astronomical interpolation of dates, relying upon crux datum $^{40}Ar/^{39}Ar$ tuff date determinations of Tuffs IID, IF, Ng'eju, IB and CFCT. Moreover, the cycle hierarchies provide timescales in those stratigraphic intervals where tuff layers are not preserved, too contaminated to allow successful dating or too widely spaced to solve stratigraphic problems.

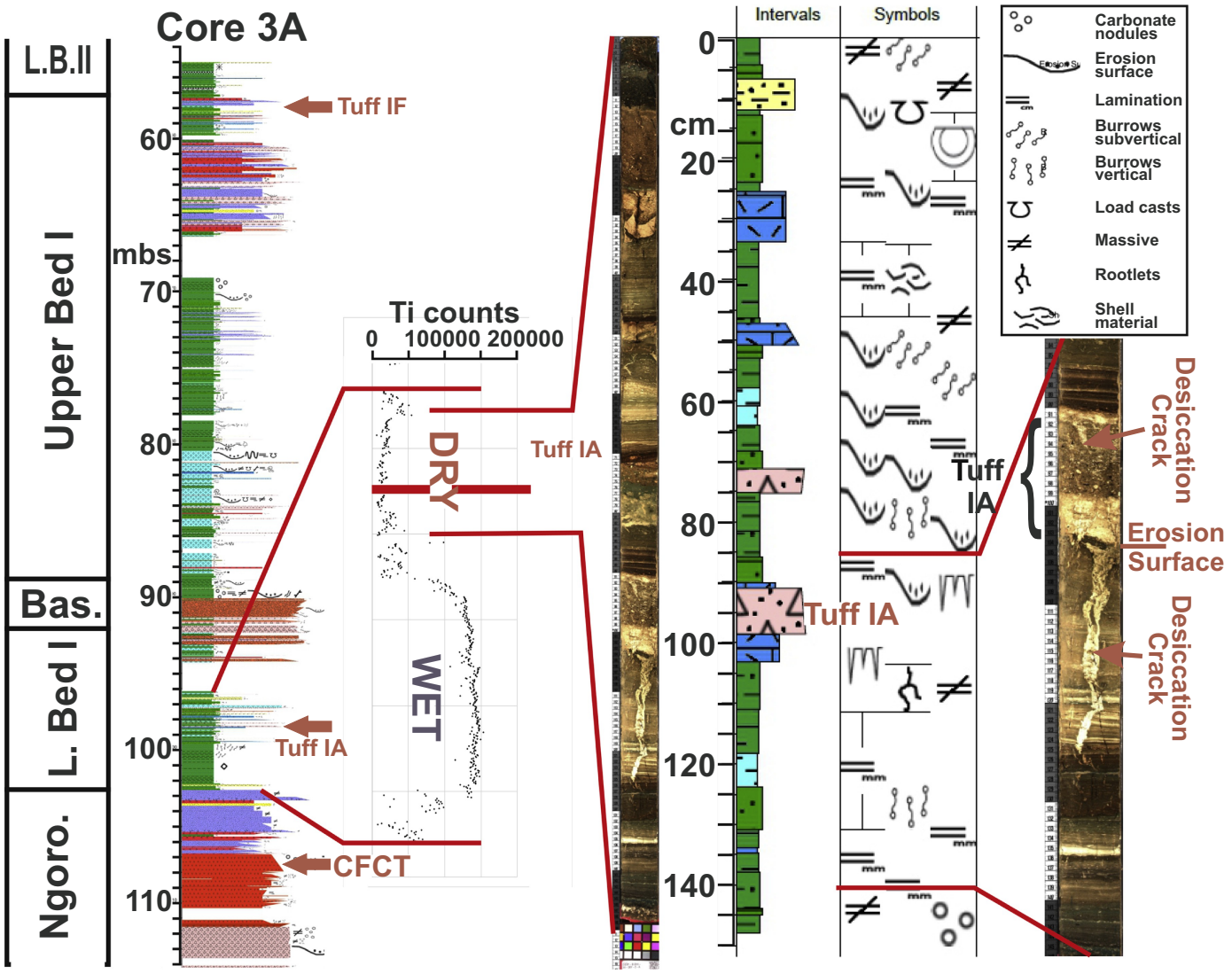

Fig. 9. Detailed positioning of Tuff IA (Core 3A) and associated desiccation features in the context of climatic changes of Lower Bed I proxied by variation in titanium input into the basin. See Fig. 2 for stratigraphic position of the section. Tuff IA was erupted during an obliquity forced dry phase in Olduvai Basin's palaeoclimatic history (see Fig. 6 for broader context). Its deposition preserved large desiccation cracks beneath, seen in Core 3A in this figure, and at outcrop, for example at Loc. 66e (Fig. 1) as figured in Habermann et al., 2016a. Elsewhere, Tuff IA is infilling a pronounced incision surface, formed during a lake lowstand. Facies legend as for Fig. 6.

7.1. Sub-Milankovitch palaeoclimatic variation Upper Bed I of Core 2A

Fig. 8 shows precessional cycles recorded in Upper Bed I and obliquital cyclic records dominating Bed II. It is significant that both of these cyclic periods were also identified by Berry (2012). However, also illustrated in Upper Bed I are cycles at a higher frequency than the precessional variation. The higher frequency signal records transgressions and regressions of Palaeolake Olduvai that would accord with the sub-Milankovitch (average ~4000–6000 a recurrence) lake-parasequential changes first recognised by Stanistreet (2012) in Upper Bed I and lowermost Bed II and subsequently identified in Bed I on the basis of TOC and carbon isotopic composition of organic matter ($\delta^{13}C_{TOC}$) variation by Colcord et al. (2018, 2019). Stanistreet et al. (2018b) and de la Torre et al. (2018a, 2018b) went further to identify parasequences in detailed facies variation in archaeological trenches at EF-HR and HWK EE in Upper and Middle Bed II respectively. Although Bed II parasequences are easily recognised at outcrop scale, particularly in lake margin settings, through drainage incision and/or palaeosol development (Stanistreet et al., 2018b), they cannot be identified in Fig. 6, due to the slower accretion rates achieved in the deposition of Bed II at the basinal depocentre compared to Bed I. It is thus the accelerated accretion rates between 2.0 and 1.8 Ma, related to enhanced basin subsidence, which allow a more extended and more highly resolved sedimentary record to be analysed.

7.2. Astronomic dating of the timing and longevity of Bed I Basalt flows

Based on the $^{40}Ar/^{39}Ar$ dates provided by the CFCT (Coarse Feldspar Crystal Tuff of Hay, 1976) and Tuff IB, the precessional cyclic periodicity suggests that the Bed I basalt would date to about 1.94 Ma. More significantly, the new record allows an estimate of how long a time was required for the eruption of the three to four basalt flows that comprise the correlative units in the Eastern Olduvai Gorge and at the Orkeri locality (Habermann et al., 2016b). Fig. 6 reveals that the three basalt flows represented as basaltic scoria-bearing layers in Borehole 3A were emplaced during a single precessional cycle (~23 kyr). More detailed correlation (Fig. 10) suggests that the three flows were produced within the timespan of two parasequences only, suggesting as little as 6 kyr to as much as 15 kyr.

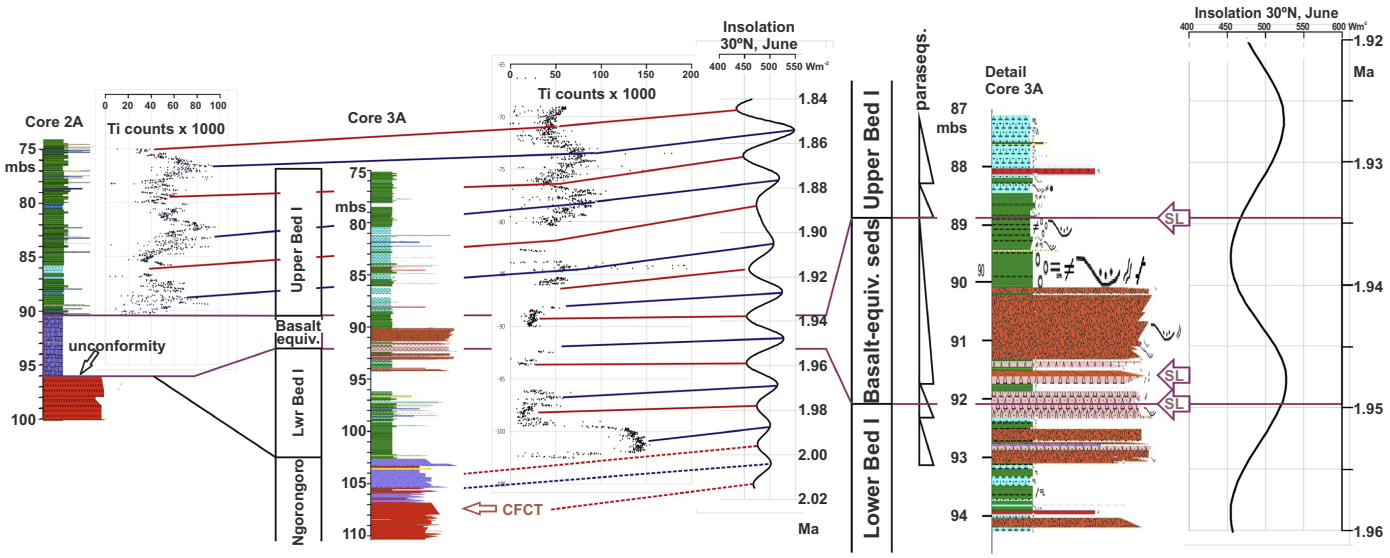

Fig. 10. Timing and duration of Bed I Basalt lava flow phase, based on Ti count climate proxy pattern, correlated to the modelled insolation curve of Laskar et al. (2004). See Fig. 2 for stratigraphic position of section. Basalt is present in Core 2A, but in Core 3A is represented by three basaltic scoriaceous layers (Red arrows labelled SL), separated by claystones, debris flows and other facies. Palaeoclimatic variation is time-bracketed by dated markers, the CFCT and Tuff IB (see Fig. 6 for context). Note that Lower Bed I sediments are missing from Core 2A, an interval represented there by a sub-Basalt unconformity. The Basalt dates astronomically to ±1.94 Ma and comprises three flow units, emplaced between ~6 kyr (based on parasequence recurrence) and 15 kyr (based on precession period). Thick gravel units (orange fill) represent olistostromes incident off the nearby Fifth Fault scarp. Facies legend as for Fig. 6, also refer to Stanistreet et al. (this volume a), symbol legend as for Fig. 9. (For interpretation of the references to colour in this figure legend, the reader is referred to the web version of this article.)

8. Conclusions

Climatic cycles have been defined in Beds I and II in the depocentre of the Olduvai Basin between Fifth and FLK Faults, using geochemical proxies derived from XRF scanning of OGCP cores 2A and 3A. The correlation of changes in Mg/Al ratios and of titanium input into Palaeolake Olduvai to palaeoclimatic variation provided important tools that could be applied as proxies in other Pleistocene and older basins. At Olduvai this extends the record of previously identified climatic forcing down to the base of Bed I and upwards to the top of Bed IV and even the Masek Beds, an order of magnitude longer than achieved in previous studies. Mg, Al, Ti cps and the Mg/Al ratio all register cyclic variations. The Bed I accretion rate is sufficiently rapid to use the element proxies to define cycles averaging 22.3 kyr periods, conforming to the ~23 kyr precessional Milankovitch band. As a consequence of accelerated accretion rates, nested transgressive and regressive variations are visible in Bed I at a higher frequency than the precessional cycles. These sub-Milankovitch climatic changes accord to previously identified Lake-parasequences, recurring on average between 4 kyr and 6 kyr. By contrast, Bed II accretion was considerably slower, so that precessional variation is not well recorded. However, cycles are defined averaging 40.4 kyr, conforming to the Milankovitch obliquity cycle at ~41 kyr period and for the first time identified in the Olduvai Basin between 1.8 and 1.3 Ma.

For illustration, there are two prime examples where climate cycles directly correspond to aridity phases registered by the sediment facies in outcrops and cores. At about 1.8 Ma a precessional cycle minimum coincided with an obliquity cycle minimum to force a phase of hyper-aridity expressed by the facies of Tuff IF. Subaerial Tuff IF facies are found in Cores 2A and 3A in widely separated locations within the basinal depocentre, indicating that Palaeolake Olduvai was dried out and/or emptied at that time. Tuff IA was deposited during another arid phase in the basin history, attested to by accompanying sedimentary structures such as deep desiccation cracks, repeated phases of incision, erosion and bioturbation by rootlets and burrows, observed both in the cores and previously in correlatable outcrops. The cyclic record can also be applied chronostratigraphically. Obliquity cycles are correlatable to the MIS Stage framework derived previously from oceanic cores. By this, MIS Stages 40 to 64 can be identified within Bed II of a basin very much inland from the Indian Ocean, whose monsoonal system dominates the East African climatic regime. The pronounced cyclicity registered would have been enhanced by the siting of the basin within the rain shadow of the Ngorongoro Volcanic Highlands. More arid phases, when the monsoonal effect was at a minimum, would have been exaggerated by the lesser ability of the weaker weather systems to penetrate the mountain range as far as the eastern Serengeti Plain. On the other hand, maximal monsoonal conditions would have more readily crossed the threshold represented by the NVH to establish much wetter phases. Moreover, the timing and longevity of the eruption of three complex Bed I Basalt flows can be estimated. The timing of emplacement was at or about 1.94 Ma and the three flows were emplaced during a period of 6 kyr to 15 kyr.

Acknowledgements

The Stone Age Institute organised and funded the Olduvai Gorge Coring Project (OGCP) and subsequent XRF scanning of the core with grants from the Kamen Foundation, the Gordon and Ann Getty Foundation, the John Templeton Foundation, the Fred Maytag Foundation, and Kay and Frank Woods. We would like to thank the Ministry of Natural Resources and Tourism (MNRT), and the Ngorongoro Conservation Area Authority (NCAA), the Tanzanian Commission for Science and Technology (COSTECH), and the Department of Antiquities for granting permission to conduct research in Tanzania. We thank Anders Noren and Kristina Brady and staff of the LacCore facility at University of Minnesota for all their support and accommodation of logging and sampling of the core. We are also very grateful to Erik Brown and Wally Lingwall of the Large Lakes Observatory, University of Minnesota, Duluth, who undertook the XRF scanning of the core. We are grateful for the detailed comments of anonymous reviewers and editor Thomas Algeo, which have improved this manuscript out of all measure. We wish to acknowledge the

analytical research of Patricia Berry, whose results from outcrops encouraged us to propose the XRF scanning of the Olduvai cores in the first place.

Appendix A. Supplementary data

Supplementary data to this article can be found online at https://doi.org/10.1016/j.palaeo.2020.109656.

References

Ashley, G.M., 2007. Orbital rhythms, monsoons, and playa lake response, Olduvai Basin equatorial East Africa (ca. 1.85–1.74 Ma). Geology 35, 1091–1094. https://doi.org/10.1130/G24163A .1.

Bamford, M.K., Stanistreet, I.R., Stollhofen, H., Albert, R.M., 2008. Late Pliocene grassland from Olduvai Gorge, Tanzania. Palaeogeography, Palaeoclimatology, Palaeoecology 257, 280–293.

Bennett, C.E., Marshall, J.D., Stanistreet, I.G., 2012. Carbonate horizons, paleosols, and lake flooding cycles: Beds I and II of Olduvai Gorge, Tanzania. J. Hum. Evol. 63, 328–341.

Berry, P., 2012. Lake Cycles and Sediments: Locality 80. Thesis, Georgia State University, Olduvai. M.Sc (63pp).

Bloemendal, J., deMenocal, P., 1989. Evidence for a change in the periodicity of tropical climate cycles at 2.4 Myr from whole-core magnetic susceptibility measurements. Nature 342, 897–899.

Calvo, J.P., Blanc-Valleron, M.M., Rodrigues-Arandia, J.P., Rouchy, J.M., Sanz, M.E., 1999. Authigenic clay minerals in continental evaporitic environments. In: Thiry, M., Simon-Coincon, R. (Eds.), Palaeoweathering. 27. pp. 129–151. https://doi.org/10.1002/9781444304190.ch5. Palaeosurfaces and Related Continental Deposits: International Society of Sedimentologists Special Publication.

Cohen, A.S., 2003. Palaeolimnology: The History and Evolution of Lake Systems. Oxford University Press (500pp).

Cohen, A.S., Arrowsmith, J.R., Behrensmeyer, A.K., Campisano, C.J., Feibel, C.S., Fisseha, S., Bedaso, Z., Lockwood, C.A., Mbua, E., Olago, D., Potts, R., Reed, K., Renaut, R., Tiercelin, J.J., Umer, M., 2009. Understanding paleoclimate and human evolution through the Hominin Sites and Paleolakes Drilling Project. Sci. Drill. 8, 60–65.

Colcord, D.E., Shilling, A.M., Sauer, P.E., Freeman, K.H., Njau, J.K., Stanistreet, I.G., Stollhofen, H., Schick, K., Toth, N., Brassell, S.C., 2018. Sub-Milankovitch paleoclimatic and paleoenvironmental variability in East Africa recorded by Pleistocene lacustrine sediments from Olduvai Gorge, Tanzania. Palaeogeogr., Palaeoclimat., Palaeoecol. 495, 284–291.

Colcord, D.E., Shilling, A.M., Freeman, K.H., Njau, J.K., Stanistreet, I.G., Stollhofen, H., Schick, K., Toth, N., Brassell, S.C. (2019, this volume). Biogeochemical records of Pleistocene environmental change at Paleolake Olduvai, Tanzania. Palaeogeogr., Palaeoclimat., Palaeoecol.

Deino, A.L., 2012. 40Ar/39Ar dating of Bed I, Olduvai Gorge, Tanzania, and the chronology of early Pleistocene climate change. In: Blumenschine, R.J., Masao, F.T., Stanistreet, I.G., Swisher, C.C. (Eds.), Five Decades after *Zinjanthropus* and *Homo habilis*: Landscape Paleoanthropology of Plio-Pleistocene Olduvai Gorge, Tanzania. J. Hum. Evol. 63, 252–273.

deMenocal, P.B., Bloemendal, J., 1995. Plio-Pleistocene subtropical African climate variability and the paleoenvironment of hominid evolution: a combined data-model approach. In: Vrba, E., Denton, G., Burckle, L., and Partridge, T., eds., Paleoclimate and Evolution With Emphasis on Human Origins. Yale University Press, New Haven, pp. 262–288.

Deocampo, D.M., 2004. Authigenic clays in East Africa: Regional trends and paleolimnology at the Plio–Pleistocene boundary, Olduvai Gorge, Tanzania. J. Paleolimnol. 31, 1–9.

Deocampo, D.M., Berry, P.A., Beverly, E.J., Ashley, G.M., Jarrett, R.E., 2017. Whole-rock geochemistry tracks precessional control of Pleistocene lake salinity at Olduvai Gorge, Tanzania: a record of authigenic clays. Geology 45, 683–686. (G38950–1). https://doi-org.proxyiub.uits.iu.edu/10.1130/G38950.1.

Domínguez-Rodrigo, M., Pickering, T.R., Baquedano, E., Mabulla, A., Mark, D.F., Musiba, C., Bunn, H.T., Uribelarrea, D., Smith, V., Diez-Martin, F., Pérez-González, A., Sánchez, P., Santonja, M., Barboni, D., Gidna, A., Ashley, G., Yravedra, J., Heaton, J.L., Arriaza, M.C., 2013. First partial skeleton of a 1.34-million-year-old *Paranthropus boisei* from Bed II, Olduvai Gorge, Tanzania. PLoS One 8, e80347.

Ferland, T.M., Colcord, D.E., Shilling, A.M., Brassell, S.C., Stanistreet, I.G., Stollhofen, H., Njau, J.K., Schick, K.D., Toth, N., Freeman, K.H, 2020 this volume this volume. Biased preservation of Pleistocene climate variability from Olduvai Gorge, Tanzania. Palaeogeogr., Palaeoclimat., Palaeoecol.

Force, E.R., 1976. Titanium contents and titanium partitioning in rocks. In: Geological Survey Professional Paper 950-A, A1-A10.

Greenwood, S.M., 2014. Mineralogy and Geochemistry of Pleistocene Volcanics at Embagai Caldera and Natron Basin, Tanzania: Potential Constraints on the Stratigraphy of Olduvai Gorge. Theses and Dissertations. Paper 497. University of Wisconsin-Milwaukee, M.Sc. Thesis (119pp).

Habermann, J.M., Stanistreet, I.G., Stollhofen, H., Albert, R.M., Bamford, M.K., Pante, M.C., Njau, J.K., Masao, F.T., 2016a. In situ ~2.0 Ma trees discovered as fossil rooted stumps, lowermost Bed I, Olduvai Gorge, Tanzania.- J. Hum. Evol. 90, 74–87.

Habermann, J.M., McHenry, L.J., Stollhofen, H., Tolosana-Delgado, R., Stanistreet, I.G., Deino, A.L., 2016b. Discrimination, correlation, and provenance of Bed I tephrostratigraphic markers, Olduvai Gorge, Tanzania, based on multivariate analyses of phenocryst compositions. Sediment. Geol. 339, 115–133.

Harris, J., Van Couvering, J., 1995. Mock Aridity and the Paleoecology of Volcanically Influenced Ecosystems. Geology 23, 593–596.

Hay, R.L., 1976. Geology of the Olduvai Gorge. California Press, Berkeley, California (203pp).

Hay, R.L., Kyser, T.K., 2001. Chemical sedimentology and paleoenvironmental history of Lake Olduvai a Pliocene lake in northern Tanzania. Geol. Soc. Am. Bull. 113, 1505–1521.

Jones, R., 1984. Heavy metals in the sediments of Llangorse Lake, Wales, since Celtic-Roman times. Verhandlungen der Internationale Vereinigung für theoretische und angewandte Limnologie 22, 1377–1382.

Jones, B.F., 1986. Clay mineral diagenesis in lacustrine sediments, in Mumpton F.A., ed., Studies in diagenesis: U.S. Geological Survey Bulletin 1578, 292–300.

Krauskopf, K.B., 1995. Introduction to Geochemistry. McGraw-Hill (647pp).

Laskar, J., Robutel, P., Joutel, F., Gastineau, M., Correia, A., Levard, B., 2004. A longterm numerical solution for the insolation quantities of the earth. Astron. Astrophys. 428, 261–285.

Leakey, M.D., 1971. Olduvai Gorge, 3. Excavations in Beds I and II, 1960 - 1963. Cambridge University Press, Cambridge (306 pp).

Lisiecki, L.E., Raymo, M.E. (2005). A Pliocene-Pleistocene stack of 57 globally distributed benthic $\delta^{18}O$ records. Palaeoceanography 20, PA1003-PA, doi:https://doi.org/10.1029/2004PA001071.

Magill, C.R., Ashley, G.M., Freeman, K.H., 2013. Ecosystem variability and early human habitats in eastern Africa. Proc. Natl. Acad. Sci. 110 (4), 1167–1174. https://doi.org/10.1073/pnas.1206276110.

McHenry, L.J., 2005. Phenocryst composition as a tool for correlating fresh and altered tephra, Bed I, Olduvai Gorge. Tanzania. Stratigraphy 2, 101–115.

McHenry, L.J., 2012. A revised stratigraphic framework for Olduvai Gorge Bed I based on tuff geochemistry. In: Blumenschine, R.J., Masao, F.T., Stanistreet, I.G., Swisher, C.C. (Eds.), Five Decades after *Zinjanthropus* and *Homo habilis*: Landscape Paleoanthropology of Plio-Pleistocene Olduvai Gorge, Tanzania. J. Hum. Evol. 63, 284–299.

McHenry L.J., Stanistreet, I.G., Stollhofen, H., Njau, J., Toth, N., and Schick, K., 2020 (This volume). Tuff fingerprinting and correlations between OGCP cores and outcrops for Pre-Bed I and BedI/II at Olduvai Gorge, Tanzania. Palaeogeography, Palaeoclimatology, Palaeoecology.

Milankovitch, M., 1941. Kanon der Erdbestrahlungen und seine Anwendung auf das Eiszeiten Problem. Roy. Serbian Acad. Spec. Pub. 133 (484pp).

Milankovitch, M., 1998. [1941]. Canon of Insolation and the Ice Age Problem. Belgrade: Zavod za Udžbenike i Nastavna Sredstva. 86-17-06619-9.

Moernaut, J., Verschuren, D., Charlet, F., Kristen, I., Fagot, M., De Batist, M., 2010. The seismic-stratigraphic record of lake-level fluctuations in Lake Challa: hydrological stability and change in equatorial East Africa over the last 140 kyr. Earth Planet. Sci. Lett. 290, 214–223.

Mollel, G.F., Swisher III, C.C., 2012. The Ngorongoro Volcanic Highland and its relationships to volcanic deposits at Olduvai Gorge and East African Rift volcanism. J. Hum. Evol. 63, 274–283.

Peters, C.R., Blumenschine, R.J., 1995. Landscape perspectives on possible land use patterns for Early Pleistocene hominids in the Olduvai Basin, Tanzania. J. Hum. Evol. 29, 321–362.

Rushworth, E., 2012. Carbonates from Olduvai Gorge. Palaeohydrology and Geochronology. Doctoral thesis, University of Liverpool, Tanzania.

Shackleton, N.J., Hall, M.A., Pate, D., 1995. Pliocene stable isotope stratigraphy of Site 846. Proc. Ocean Drilling Program, Sci. Results 138, 337–355.

Shaw, H.R. (1980). The fracture mechanisms of magma transport from the mantle to the surface. In: Hargraves, R.B. (Ed.): *Physics of magmatic processes*, 64, pp. 201-264. Princeton University Press, Princeton, New Jersey. 565pp.

Shilling, A.M., Colcord, D.E., Karty, J., Hansen, A., Freeman, K.H., Njau, J.K., Stanistreet, I.G., Stollhofen, H., Schick, K.D., Toth, N., Brassell, S.C, 2019 this volume this volume. Biomarker evidence for environmental changes of Pleistocene Lake Olduvai during the transitional sequence that encompasses Tuff 1B (~1.848 Ma). Palaeogeography, Palaeoclimatology, Palaeoecology 532, 109267. https://doi.org/10.1016/j.palaeo.2019.109267.

Stanistreet, I.G., 2012. Fine resolution of early hominin time, Beds I and II, Olduvai Gorge, Tanzania. J. Hum. Evol. 63 (2), 300–308. https://doi.org/10.1016/j.jhevol.2012.03.001.

Stanistreet, I.G., Stollhofen, H., Njau, J.K., Farrugia, P., Pante, M.C., Masao, F.T., Albert, R.M., Bamford, M.K., 2018a. Lahar inundated, modified and preserved 1.88 Ma early hominin (OH24 and OH56) Olduvai DK site. J. Hum. Evol. 116, 27–42.

Stanistreet, I.G., McHenry, L.J., Stollhofen, H., De La Torre, I., 2018b. Bed II Sequence stratigraphic context of EF-HR and HWK EE archaeological sites, and the Oldowan/Acheulean succession at Olduvai Gorge, Tanzania. J. Hum. Evol. 120, 19–31.

Stanistreet, I.G., Stollhofen, H., Deino, A., McHenry, L., Toth, N., Schick, K., Njau, J., 2020a, this volume. New Olduvai Basin stratigraphy and stratigraphic concepts revealed by OGCP cores into the Palaeolake Olduvai depocentre, Tanzania. Palaeogeogr., Palaeoclimat., Palaeoecol.

Stanistreet, I.G., Doyle, C., Hughes, T., Rushworth, E.R., Stollhofen, H., Toth, N., Schick, K., Njau J., 2020b, this volume. Changing depocentre environments of Palaeolake Olduvai and carbonates as marker horizons for hiatuses and lake-level extremes. Palaeogeogr. Palaeoclimatol. Palaeoecol.

Stollhofen, H., Stanistreet, I., 2012. Plio-Pleistocene synsedimentary fault compartments, foundation for the eastern Olduvai Basin paleoenvironmental mosaic, Tanzania. J. Hum. Evol. 63, 309–327.

Stollhofen, H., McHenry, L., Stanistreet, I.G., Mollel, G., Blumenschine, R., Masao, F.T., 2008. Fingerprinting facies of the Tuff IF marker, with implications for early hominin

palaeoecology, Olduvai Gorge, Tanzania. Palaeogeography, Palaeoclimatology, Palaeoecology 259, 382–409.

de la Torre, I., Albert, R.M., Macphail, R., McHenry, L.J., Pante, M.C., Rodríguez- Cintas, A., Stanistreet, I.G., Stollhofen, H., 2018a. The contexts and early Acheulean archaeology of the EF-HR palaeo-landscape (Olduvai Gorge, Tanzania). J. Hum. Evol. 120, 274–297.

de la Torre, I., Albert, R.M., Arroyo, A., Macphail, R., McHenry, L.J., Mora, R., Njau, J.K., Pante, M.C., Rivera-Rondon, C.A., Rodríguez-Cintas, A., Stanistreet, I.G., Stollhofen, H., Wehr, K., et al., 2018b. New excavations at the HWK EE site: archaeology, paleoenvironment and site formation processes during late Oldowan times at Olduvai Gorge, Tanzania. Journal of Human Evolution 120, 140–202.

Verschuren, D., Sinninghe Damsté, J., Moernaut, J., Kristen, I., Blaauw, M., Fagot, M., Haug, G., van Geel, B., De Batist, M., Barker, P., Vuille, M., Conley, D., Olago, D.O., Milne, I., Plessen, B., Eggermont, H., Wolff, C., Hurrell, E., Ossebaar, J., Lyaruu, A., van der Plicht, J., Cumming, B.F., Brauer, A., Rucina, S.M., Russell, J.M., Keppens, E., Hus, J., Bradley, R.S., Leng, M., Mingram, J., Nowaczyk, N.R., 2009. Half-precessional dynamics of monsoon rainfall near the East African equator. Nature 462, 637–641.

Webster, D.M., Jones, B.F., 1994. Paleoenvironmental implications of lacustrine clay minerals from the Double Lakes Formation, southern High Plains, Texas, in Renaut, R.W., and Last, W.M., eds. Sedimentology and Geochemistry of Modern and Ancient Saline Lakes: SEPM (Society for Sedimentary Geology) Special Publication 50, 159–172. https://doi.org/10.2110/pec.94.50.0159.